

RADIATION-RESISTANT DEVICE PHENOMENA

By William C. Follmer and Dr. Arnold Berman

December 1964

GPO PRICE \$ _____

OTS PRICE(S) \$ _____

Hard copy (HC) 3.00

Microfiche (MF) .75

FACILITY FORM 402

N65 17886
(ACCESSION NUMBER)

72
(PAGES)

CR 60944
(NASA CR OR TMX OR AD NUMBER)

(THRU)

1
(CODE)

09
(CATEGORY)

Prepared Under Contract No. NASW-997 by

PHILCO CORPORATION
A Subsidiary of Ford Motor Company
Applied Research Laboratory
Blue Bell, Pennsylvania

NATIONAL AERONAUTICS AND SPACE ADMINISTRATION

TABLE OF CONTENTS

Section	Page
SUMMARY	1
INTRODUCTION	1
ELECTRON TRANSPORT THROUGH THIN FILMS	3
Experimental Studies of Energetic Electrons	3
Experimental Details	5
Electron gun	5
Diodes	8
Circuitry	8
REACTIVELY DEPOSITED ALUMINUM OXIDE	11
Reactive Evaporation	11
Deposition Technique	12
Electrical Evaluation	12
Facilities for the Production of Reactively Evaporated Aluminum-Oxide Films	13
Vacuum system and drybox assembly	13
Oxygen-pressure monitor and control system	13
Deposition controller and mass monitor	14
Vacuum system accessories	14
Initial sample masking	14
Substrate material	15

Libraries of contractors and of other qualified requesters may obtain additional copies of this report by submitting NASA Form 492 directly to:

Scientific and Technical Information Facility
P. O. Box 5700
Bethesda, Maryland 20014

LIST OF ILLUSTRATIONS

Figure		Page
1	Energy Diagram of Electron Transport Experiment	4
2	Simplified Experimental Steup for Electron Transport Measurements	6
3	Low-Energy Electron Gun	7
4	Current-Voltage Characteristics of Low-Energy Electron Gun	9
5	Collector Diode	10
6	Typical Mask Patterns	16

LIST OF APPENDIXES

Appendix		Page
A	Vacuum System and Drybox Assembly	17
B	Pressure Monitor and Oxygen-Pressure Control System	21
C	A Resonant Quartz Microscale (R. Q. M.) Deposition-Control System	32

SUMMARY

17886
425
This report describes the initial work expended with regard to setting up the equipment necessary to perform fundamental measurements on energetic electron transport through thin metal films, and the development of reactively evaporated aluminum-oxide films for use in thin-film devices.

An experiment utilizing a special low-energy electron gun as a source of energetic electrons has been set up in an ultrahigh-vacuum system and is now undergoing final tests before the start of measurements on the attenuation length of energetic electrons in thin gold films.

A majority of the facilities required for the controlled production of reactively evaporated aluminum-oxide films have been designed and constructed during the first reporting period. These facilities include a high-vacuum system and drybox assembly to prevent film contamination, a resonant quartz microscale (R.Q.M.) deposition rate monitor and controller, and an oxygen-pressure servo control system.

Author

INTRODUCTION

The need for highly reliable solid-state electronic components for use in the space program has led to an intensive investigation of devices capable of performing active circuit functions and offering improved resistance to the radiation damage known to occur in the space environment. This investigation has shown that majority carrier devices in which the active process takes place in an extremely small volume will produce the desired improvement in radiation resistance. At present there are two approaches to such a radiation-resistant device: the metal-base transistor and the field-effect transistor. Both approaches offer the possibility of improved performance levels in addition to the desired improvement in radiation resistance. Philco has been conducting a research program aimed at developing devices of each of the above classes. Substantial progress has been made, both in the theoretical understanding of these structures and in the technology required to implement them.

The metal-base transistor (MBT) approach to a radiation-resistant device makes use of the transport of energetic electrons across thin metal films. Philco has been active in the study of such triode structures for

SUMMARY

17886
485
This report describes the initial work expended with regard to setting up the equipment necessary to perform fundamental measurements on energetic electron transport through thin metal films, and the development of reactively evaporated aluminum-oxide films for use in thin-film devices.

An experiment utilizing a special low-energy electron gun as a source of energetic electrons has been set up in an ultrahigh-vacuum system and is now undergoing final tests before the start of measurements on the attenuation length of energetic electrons in thin gold films.

A majority of the facilities required for the controlled production of reactively evaporated aluminum-oxide films have been designed and constructed during the first reporting period. These facilities include a high-vacuum system and drybox assembly to prevent film contamination, a resonant quartz microscale (R.Q.M.) deposition rate monitor and controller, and an oxygen-pressure servo control system.

Author

INTRODUCTION

The need for highly reliable solid-state electronic components for use in the space program has led to an intensive investigation of devices capable of performing active circuit functions and offering improved resistance to the radiation damage known to occur in the space environment. This investigation has shown that majority carrier devices in which the active process takes place in an extremely small volume will produce the desired improvement in radiation resistance. At present there are two approaches to such a radiation-resistant device: the metal-base transistor and the field-effect transistor. Both approaches offer the possibility of improved performance levels in addition to the desired improvement in radiation resistance. Philco has been conducting a research program aimed at developing devices of each of the above classes. Substantial progress has been made, both in the theoretical understanding of these structures and in the technology required to implement them.

The metal-base transistor (MBT) approach to a radiation-resistant device makes use of the transport of energetic electrons across thin metal films. Philco has been active in the study of such triode structures for

several years, and a comprehensive theory for the performance of these devices has been developed. Fundamental measurements programs have been under way for some time to determine the attenuation length of energetic electrons in various metals and also to evaluate the collection efficiency of various collector structures.

Studies are also being conducted to develop the needed technology for the production of very thin, compact, insulating films to be used in active thin-film devices. Two such methods are known; namely, gaseous anodization¹ and reactive evaporation.^{2,3} Both of these processes are capable of producing the desired film dimensions. The former method has the disadvantage that such films can be produced only on valve metals such as aluminum, tantalum, etc. It is, however, reproducible and uniform. The latter method, with which Philco has had considerable success in recent months, is theoretically applicable to film deposition on any metal or insulator, although the work done to date has been limited to aluminum substrates. While this method shows promise of also being extremely reproducible, more studies are necessary to prove this point.

Once the proper techniques have been developed for the production of these thin insulating films, it is necessary to evaluate their use in thin-film active devices. This will be done as part of Philco's fundamental measurements program. In this way, complete characterization of the individual film elements to be used in thin-film active devices can be obtained so that the experimental results obtained on triode structures can be better evaluated and understood.

ELECTRON TRANSPORT THROUGH THIN FILMS

The objective of this part of the contract is to study the transport of energetic electrons across thin metal films, and the collection of these electrons. Under a previous program, Philco has conducted extensive fundamental studies regarding the mean free path of energetic electrons in thin films, and the collection efficiency of metal-insulator and metal-semiconductor interfaces. Results of these theoretical studies have been reported.⁴ They show that the problems of transport and collection are the fundamental processes that are most important if one is to successfully operate a metal-base transistor. This preliminary work has also suggested an experimental technique which should provide information regarding both the mean free path and the collection efficiency. It is this experiment which will be pursued during the course of this contract.

Experimental Studies of Energetic Electrons

It is desired to examine the transport of a directed beam of fast electrons through a thin metal film and their collection at a metal-semiconductor barrier. To make this study a gold-silicon diode will be bombarded by an external beam of low-energy electrons. The diode will act in a way similar to the collector element of a metal-base transistor, but the use of an external electron beam will avoid the ambiguities of interpretation which beset an all-thin-film device.

An energy diagram of the experiment is shown in Figure 1. The electrons emitted from the tungsten cathode will have an energy ξ above the Fermi level of the gold film. The minimum value of ξ will be determined by the gold work function ϕ_2 . This can be reduced to about 1.8 volts by a monomolecular layer of BaO. Upon entering the gold film, the electrons will acquire an additional energy of several volts, with momentum directed normal to the film. Most of this kinetic energy will be lost upon entering the conduction band of the silicon. The very small critical angle of collection will ensure that any collision in the gold base layer will prevent collection. Those electrons that do not collide in the gold film and do not back-scatter from the silicon will be observed as a collection current. The remaining electrons will return to the cathode through the base layer. By measuring the fraction collected as a function of film thickness, the total mean free path can be determined and the transport efficiency separated from the effects of collection efficiency. This will be done over a range of electron energies which can hopefully be extrapolated to the low-energy limit.

LEGEND:

- ϕ_1 : WORK FUNCTION OF TUNGSTEN.
 ϕ_2 : REDUCED WORK FUNCTION OF GOLD.
 $\xi = \phi_1 - eV$

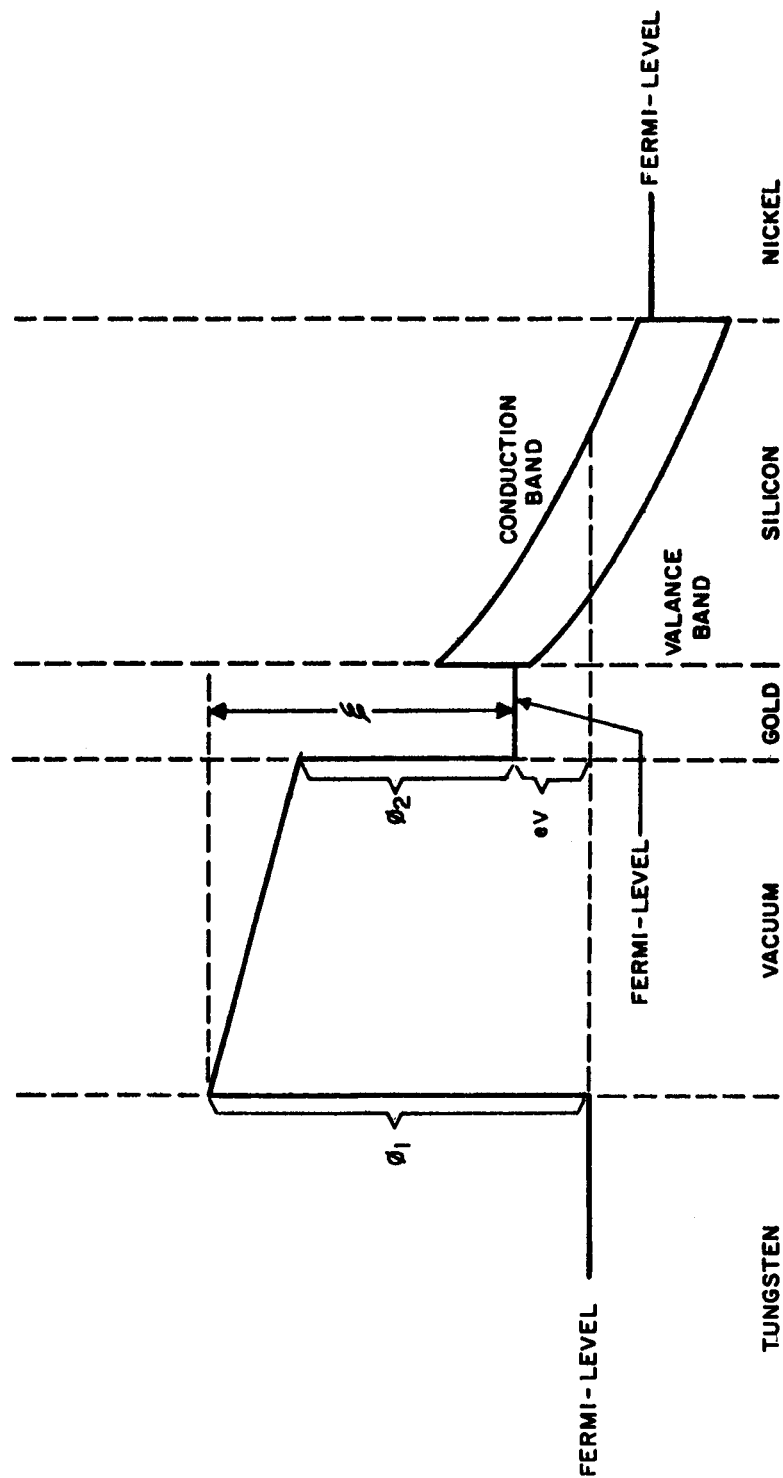


Figure 1. Energy Diagram of Electron Transport Experiment

When the details of this experiment have been worked out, it can be used as a tool for measuring the transport efficiency of any metal base and the collection efficiency of any interface.

Experimental Details

Electron gun. - Because of the requirement of a very-low-energy electron beam, the space charge will severely limit the magnitude of the beam current available. To partially compensate for this limitation, both the cathode and diode areas are made large, about one cm^2 . The cathode disk is heated by electron bombardment at high voltage from the rear. This allows heating by a relatively small current so that large voltage drops do not develop along the cathode and make the electron energy uncertain.

The electron energy \mathcal{E} is known from the tungsten work function and the applied voltage. The cathode may be heated to 2000°C to expose a clean surface whose work function is well known. The experiment is carried out at pressures of about 10^{-8} torr to keep the surface clean. The gun has gone through various stages of design during this experiment. Figure 2 shows schematically the present design which was assembled and tested during the past quarter. A photograph of the actual gun is shown in Figure 3.

The cathode is separated from the sample by about 2 inches to prevent heating of the sample. The diameter of the gun must be correspondingly large to transmit the electron beam. This separation results in severe space-charge limitation of the beam current. To circumvent this condition, an accelerating grid is mounted at the end of the gun and the space charge is confined to the small grid-sample separation.

The shield, which is closely spaced to the cathode, prevents electrons from the tantalum cathode holder, as well as ions created in the vicinity of the filament, from entering the cathode beam. These ions, which manifested themselves in a reverse current at retarding potentials, plagued earlier gun designs.

The focusing electrode serves to confine the beam to the incident side of the diode. This is important, since it is expected that collection efficiencies as small as 10^{-4} will be measured. The beam current displays a sharp maximum as the focusing voltage, V_F , is varied. This makes a convenient control to modulate the beam current.

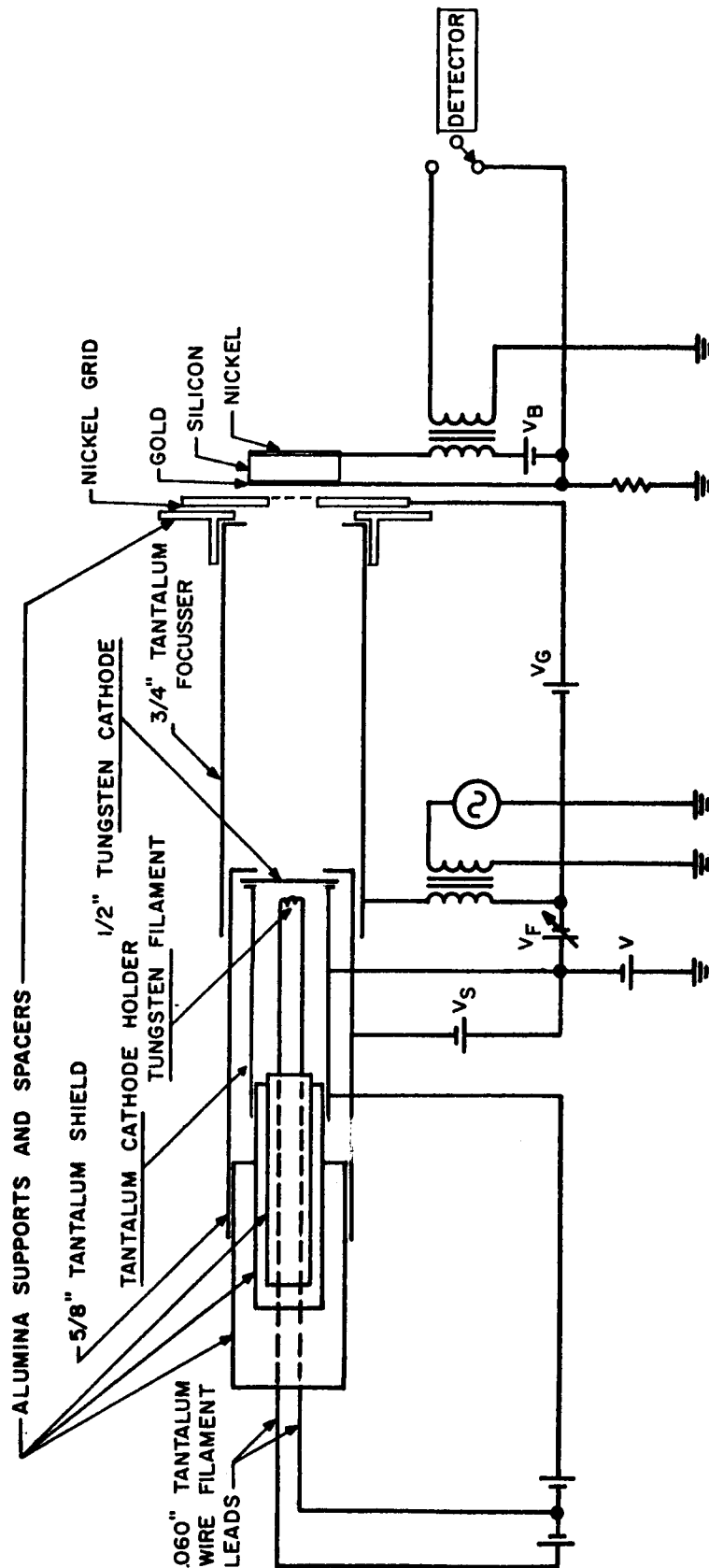


Figure 2. Simplified Experimental Setup for Electron Transport Measurements

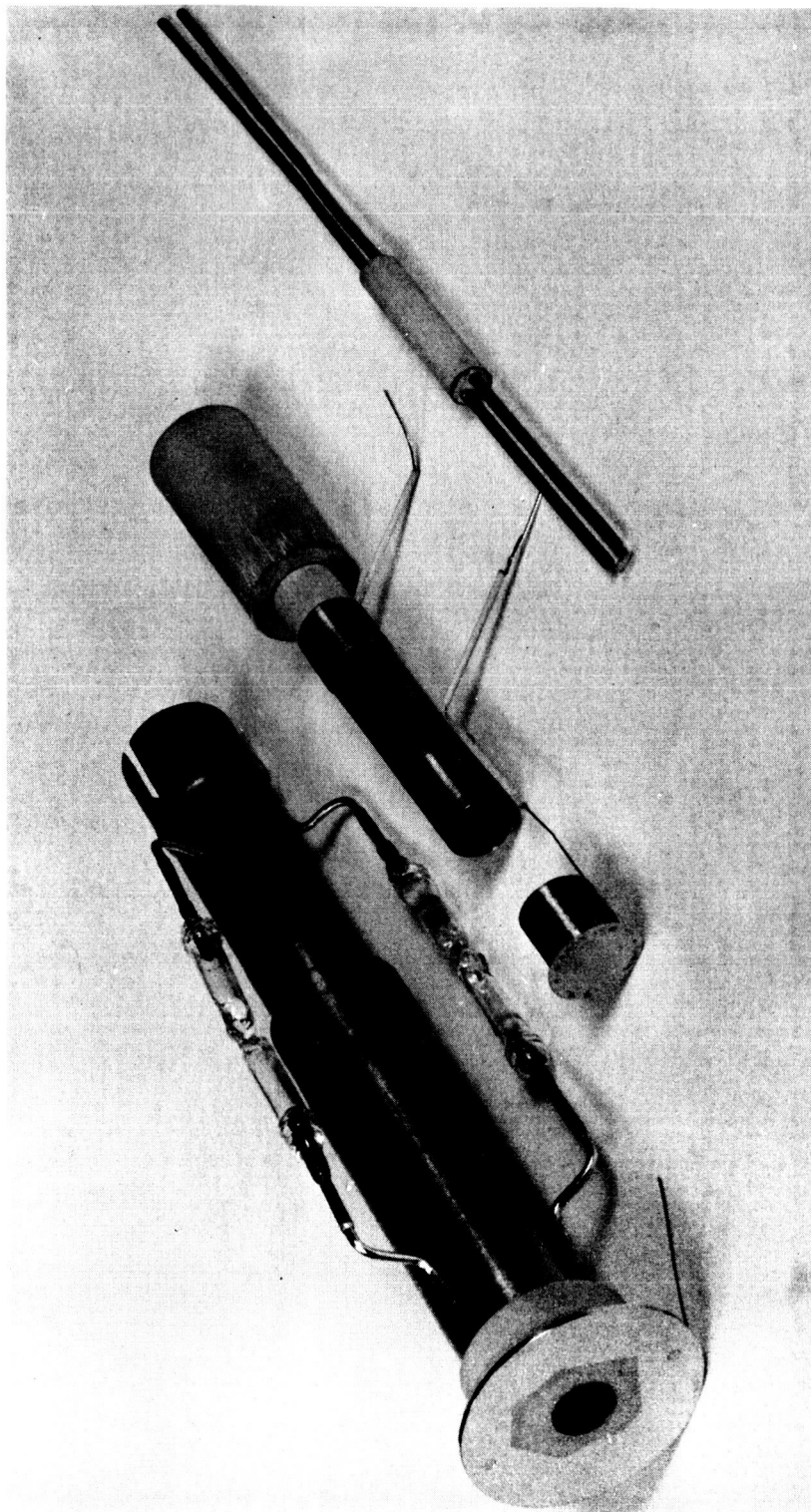


Figure 3. Low-Energy Electron Gun

Current-voltage characteristics are shown in Figure 4 for various values of grid voltage V_G . In these curves, V_F and V_S are optimized for a maximum beam current.

Diodes. - The diodes are made by evaporating a gold film onto a silicon blank which has been prepared as shown in Figure 5. Gold was chosen for the initial work because of its chemical stability, known phonon mean free path, and anticipated electron-electron mean free path, and because of previous work done on reducing the gold work function with barium oxide. A resonant quartz microscale (R.Q.M.) will be used to monitor the mass per unit area of both the vacuum-deposited gold film and the barium-oxide monolayer.

The nickel makes ohmic contact to the silicon; the gold layer provides contact to the gold film to be evaporated onto the exposed silicon; and the oxide layer insulates the gold contact layer from the silicon.

A number of silicon blanks were prepared during the reporting periods, but they proved to have intermittent electrical shorts through the oxide layer. Another group is now being prepared under more careful conditions to prevent the reoccurrence of this problem.

Circuitry. - In order to measure collection currents as small as 10^{-11} ampere, sensitive detection methods and a high degree of isolation from spurious coupling are required. The grid, which is kept at a low impedance to ground, serves to capacitively decouple the diode from the focuser and thus prevent stray currents in the absence of a beam current.

The circuit shown in Figure 2 has been assembled and preliminary tests made. With narrow banding, the small currents can be measured with the PARJB5 detector.

LEGEND:

$T_C = 1375^\circ\text{C}$

$V_F = 0.5 \text{ VOLTS}$

$V_S = 0$

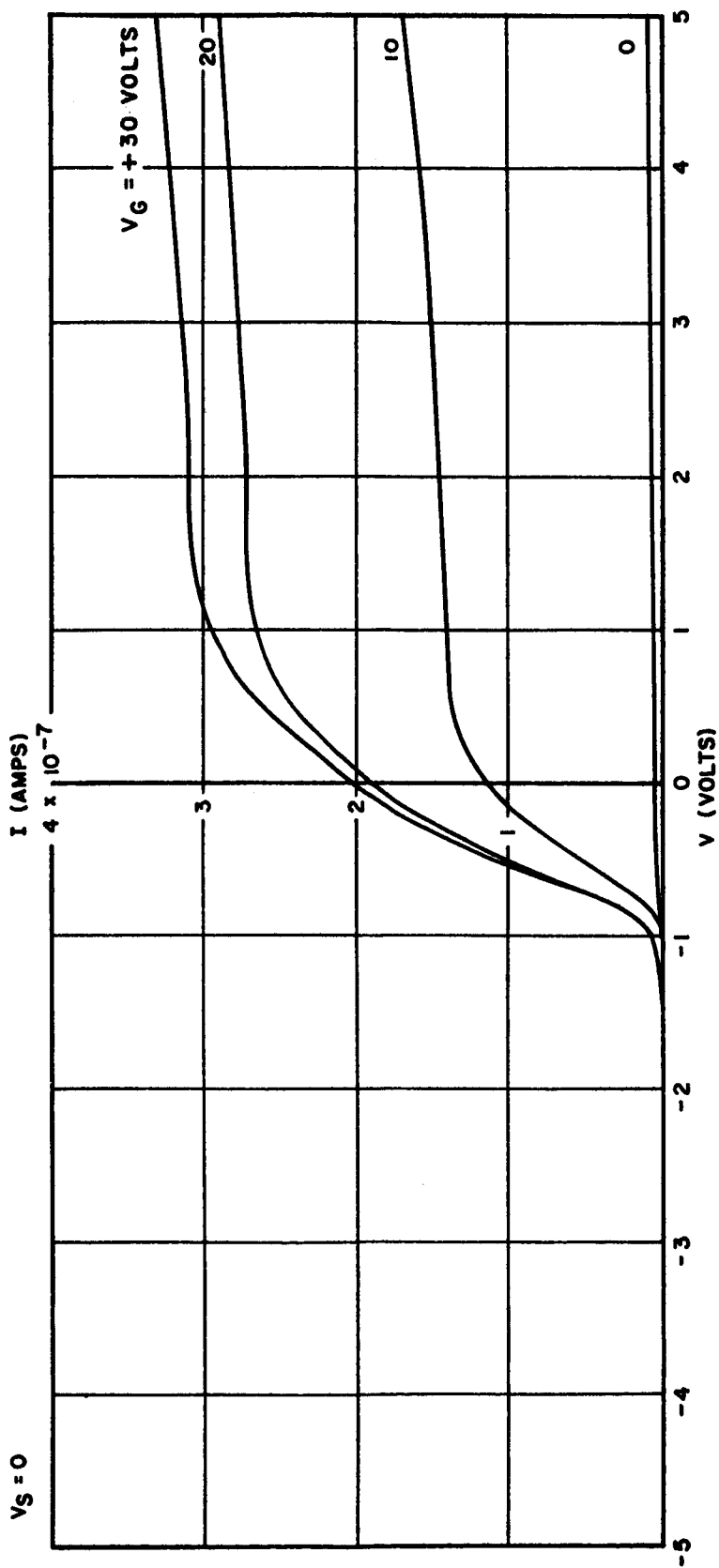


Figure 4. Current-Voltage Characteristics of Low-Energy Electron Gun

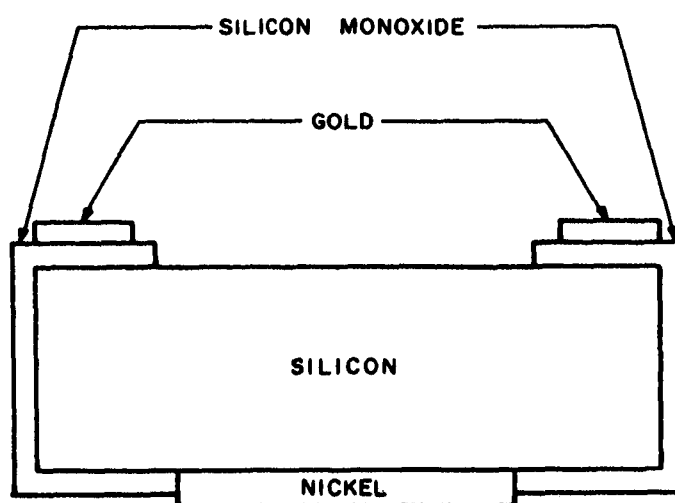


Figure 5. Collector Diode

REACTIVELY DEPOSITED ALUMINUM OXIDE

Reactive Evaporation

The high resistivity, high breakdown strength, and stability of aluminum oxide have encouraged its investigation as a possible candidate for a thin-film insulator. Early work on aluminum oxide utilized the natural oxide as an insulating barrier. This technique did not provide a reproducible, high-field insulator. There are at least two techniques that have been shown to produce excellent insulating films. These are the gaseous anodization¹ of a previously deposited film and the reactive evaporation of aluminum oxide.^{2,3} The reactive evaporation technique has the advantage in that the insulating film can be deposited upon any desired substrate, and for this reason is being studied for application to thin-film active-device fabrication.

To obtain reactively evaporated aluminum films, pure aluminum is evaporated in a background pressure of oxygen of approximately 1×10^{-3} mm. The deposition rate is purposely kept low so that the aluminum deposited may be continuously oxidized by the oxygen present in the system. A typical Al_2O_3 deposition rate for the initial work was 24×10^{-9} grams per cm^2 per second. This corresponds to 3×10^{14} aluminum atoms per second per square cm. At an oxygen pressure of 10^{-3} mm, one can calculate that the resulting oxygen molecule impact rate is 6×10^{15} impacts per cm^2 per second. It can also be calculated⁴ that the mean free path of the evaporated aluminum is of the order of 8 centimeters at 10^{-3} mm oxygen. With a source-to-substrate spacing of less than the mean free path, it is then reasonable to assume that the majority of the oxidation occurs after the aluminum atoms have condensed on the substrate. It can be seen from these calculations that the degree of oxidation in the deposited film will depend upon the oxygen pressure and the deposition rate. Previous experimental work has shown that films of resistivity varying from essentially that of pure aluminum, 10^{-5} ohm per cm, to that of aluminum oxide, 10^{14} ohms per cm, can be prepared by varying the oxygen pressure and/or the deposition rate. Thus, the requirement exists for tight control of the deposition rate and oxygen pressure if one desires films of known and controllable composition.

In addition to these problems in preparation, aluminum oxide absorbs a substantial amount of water vapor if exposed to a wet gas. This water-vapor absorption could seriously affect the electrical characteristics

of the insulating film. It is therefore important that the films be protected from contamination. Further, as in any film work, dust contamination is a serious problem and must be eliminated. These considerations have led to the development of the following experimental procedure for the study of reactively evaporated films of aluminum oxide.

Deposition Technique

The preparation of aluminum-oxide samples for electrical evaluation will consist of three major steps. In the first step, metal electrodes will be evaporated onto the glass substrates, using conventional metal evaporation techniques and contact masks to obtain the desired patterns.

The glass substrates with the previously deposited metal electrodes will then be placed in a second mask and re-installed in the vacuum system. Pure aluminum metal will be evaporated from a tungsten boat in the vacuum system that has previously been evacuated to below 10^{-6} mm Hg and then back-filled to approximately 10^{-3} mm Hg with oxygen. During evaporation, while oxygen continuously flows through the system, the servo-control leak will maintain the pressure at the preset level.

The resulting film of aluminum oxide is deposited through the aluminum contact mask onto the glass substrates. The R.Q.M. sample oscillator mounted adjacent to the substrates also receives a film deposit. This deposit is monitored and provides the signals that are used to control the deposition rate.

Finally, counterelectrodes are applied to the aluminum oxide by a second metal evaporation.

The glass substrates will then be scribed and the individual samples mounted in TO-5 headers for electrical evaluation. During the encapsulation procedure the samples will be maintained in a dry atmosphere of nitrogen gas.

Electrical Evaluation

Initially, films will be measured for resistivity as a function of temperature, dielectric strength, and dielectric constant.

Resistivity will be obtained from a four-terminal resistance measurement and from multiple-beam interferometer thickness measurements. The thickness measurements will be correlated with the R.Q.M. mass measurements to obtain an indication of the film density.

A low-frequency capacity bridge (100 kc) will provide semiprecision measurements of the capacity for dielectric-constant calculations. Capacity-type samples will also be utilized in the measurement of breakdown voltage.

Facilities for the Production of Reactively Evaporated Aluminum-Oxide Films

Practically the entire effort during this reporting period was devoted to procuring, designing, and assembling the necessary facilities required for the production of reactively evaporated aluminum-oxide films. The following paragraphs summarize these facilities and their present status. Detailed descriptions of these facilities are included as Appendixes A, B, and C.

Vacuum system and drybox assembly. - The aluminum-oxide films will be prepared in an oil-diffusion pumped-vacuum system capable of ultimate pressures of 3×10^{-7} mm. This system utilizes a liquid-nitrogen cooled cold trap to prevent back-streaming of the pumping oil. A drybox unit has been received and is now being installed on the vacuum system to eliminate the water-vapor contamination of the prepared films. This drybox unit will be continuously flushed with nitrogen gas obtained from the boil-off of liquid nitrogen. A detailed description of this assembly is given in Appendix A.

To further reduce the possibility of dust contamination, an absolute filter and recirculating system is planned for installation on the drybox.

The vacuum-system/drybox assembly is mechanically complete, but the electrical circuits and gas feeds are yet to be installed.

Oxygen-pressure monitor and control system. - The oxygen-pressure monitor and control system utilizes a commercial ionization gauge, Veeco R31-X, as the pressure-monitoring instrument. The recorder output of this instrument is coupled to the pressure-controller electronics section which provides the necessary signals to regulate the oxygen pressure in the system with a servo-driven leak valve. A Leeds and Northrup chart

recorder is also connected to the recorder output of the pressure gauge to provide a continuous record of the system pressure. The oxygen-pressure control system is provided with interlocks to prevent inappropriate opening of the leak valve. The ionization gauge, pressure-control electronics, and chart recorder are mounted in a standard relay rack located adjacent to the vacuum system. A detailed description of this assembly is contained in Appendix B.

This unit is completed and will be tested upon completion of the vacuum system and drybox assembly.

Deposition controller and mass monitor. - The deposition controller and mass monitor utilizes the shift in resonant frequency of a quartz crystal when a sample of the film is deposited on the surface of the crystal.^{5,6,7} The shift in resonant frequency of the crystal has been shown to be proportional to the mass per unit area of the deposited film. This frequency shift is monitored and provides the information on the deposited mass which is proportional to film thickness, assuming that the density is constant. This mass signal is also differentiated and provides the deposition-rate signal. A servo system compares the deposition-rate signal to a reference signal and adjusts the evaporator temperature via a servo-motor-driven variac to obtain the desired rate. A detailed description of the resonant quartz microscale (R.Q.M.) deposition-rate controller can be found in Appendix C. This equipment is at the present time completely designed and about 95 percent constructed, awaiting only the delivery of some small components to allow completion. The deposition-rate controller and mass-monitor components are mounted in a second relay rack which will be located adjacent to the vacuum system.

A two-channel strip-chart recorder is needed to provide continuous records of deposition rate and deposited mass. Such a unit has been on order for some time.

Vacuum system accessories. - A water-cooled support for the in-vacuum components has been designed and the commercial elements ordered. This unit will provide a single mounting post to which the R.Q.M. sample oscillator, substrate holder, substrate temperature monitor, and shutter will be mounted. This single post will offer a maximum of versatility while occupying a minimum volume in the vacuum system.

Initial sample masking. - A set of three masks has been designed and is now in drafting for detailed design which will provide samples suitable for

resistivity, dielectric constant, breakdown-field, and high-field mobility measurements. Figure 6, parts A, B, and C, are sketches of the preliminary mask design. Aluminum has been chosen as the mask material because of its ease of machinability.

Substrate material. - Previous work in vacuum-deposited thin films has indicated that microscope slide cover glass, Corning type No. 2, has very smooth surfaces and is suitable for the deposition and study of thin films. In addition, these glass substrates are easily scribed and broken into individual samples which are suitable for encapsulation using standard transistor packages. This encapsulation will provide further protection from contamination while the films are characterized.

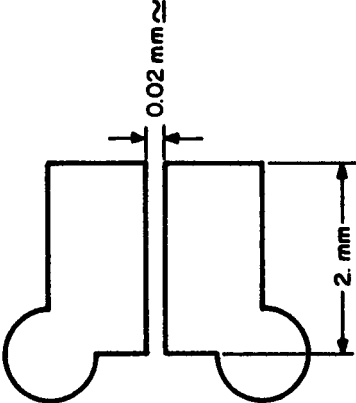
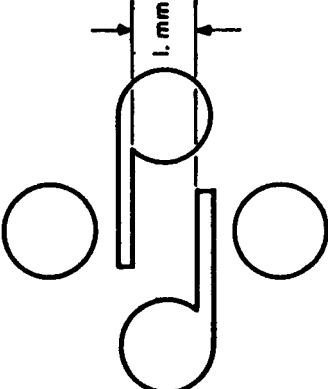
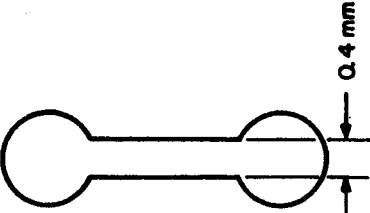

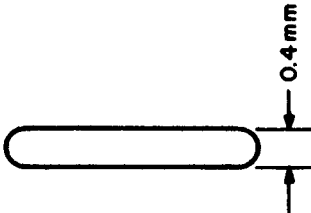


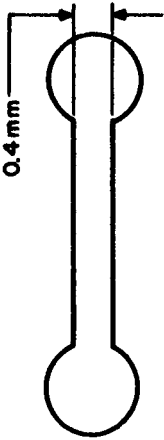
	FET	4-TERMINAL RESISTOR	CAPACITOR
MASK NO. 1 BOTTOM ELECTRODES			
MASK NO. 2 MATERIAL TO BE TESTED			
MASK NO. 3 COUNTERELECTRODES		NONE	

Figure 6. Typical Mask Patterns

APPENDIX A

VACUUM SYSTEM AND DRYBOX ASSEMBLY

Vacuum-System Components

A Kinney KC 15 mechanical pump is used as the roughing pump and backing pump for a CVC PMCU-721 oil-diffusion pump. The diffusion pump is connected through a CVC BCN liquid-nitrogen-cooled chevron cold trap and a Temascal high-vacuum valve to the modified 16-inch Kinney baseplate. The baseplate unit now contains thirteen 3/4-inch nominal diameter holes through which the vacuum-system accessories will be installed.

Veeco SV62S solenoid valves are used for roughing and backing. Initially, a 14-inch-diameter glass bell jar will be used. A counterbalanced, motor-driven, bell-jar hoist completes the vacuum-system installation. The electrical and gas-feed connections are shown in Figures A-1 and A-2.

The Drybox Unit

A specially designed plexiglass drybox (Hydrovoid) has been obtained from Air Control. This unit provides both a controlled atmosphere and protection from dust contamination for the prepared samples. The bell-jar unit is sealed with a flexible bellows to allow raising the bell jar. The sliding hand-port assembly incorporated into this unit further increases its versatility.

Nitrogen gas, obtained from the evaporation of liquid nitrogen, is continuously fed into the drybox through a pressure regulator to maintain a positive internal pressure. A needle-valve-and-flow-meter unit mounted on the vent line provides both monitoring and control of the gas-flow rate.

A future addition to the system will be an absolute filter in a recirculating system to remove any remaining dust in the drybox. Details of the gas feed are shown in Figure A-2 referred to previously. Figure A-3 is a photograph of the complete vacuum system and drybox assembly.

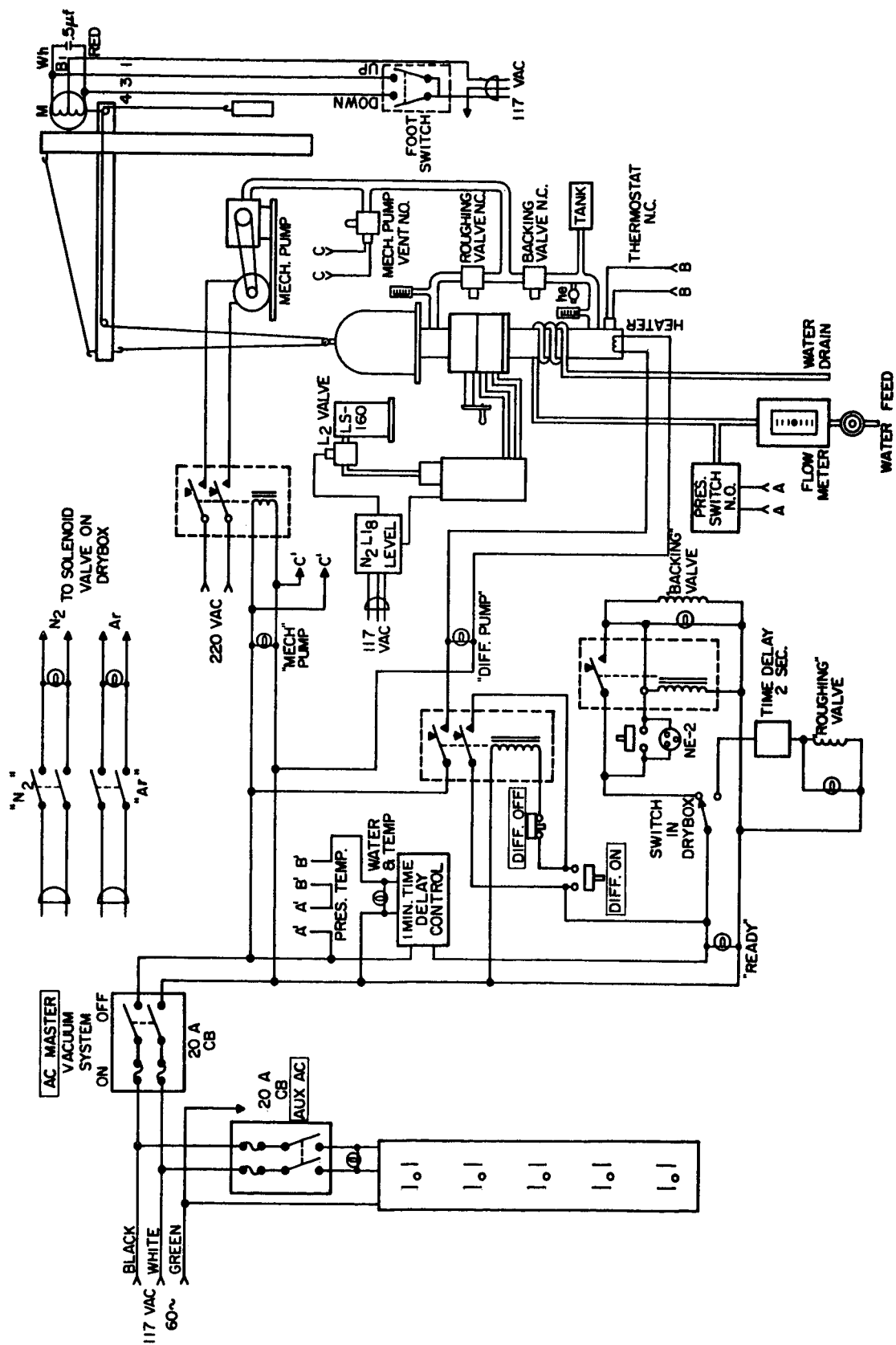


Figure A-1. Vacuum System AC Schematic

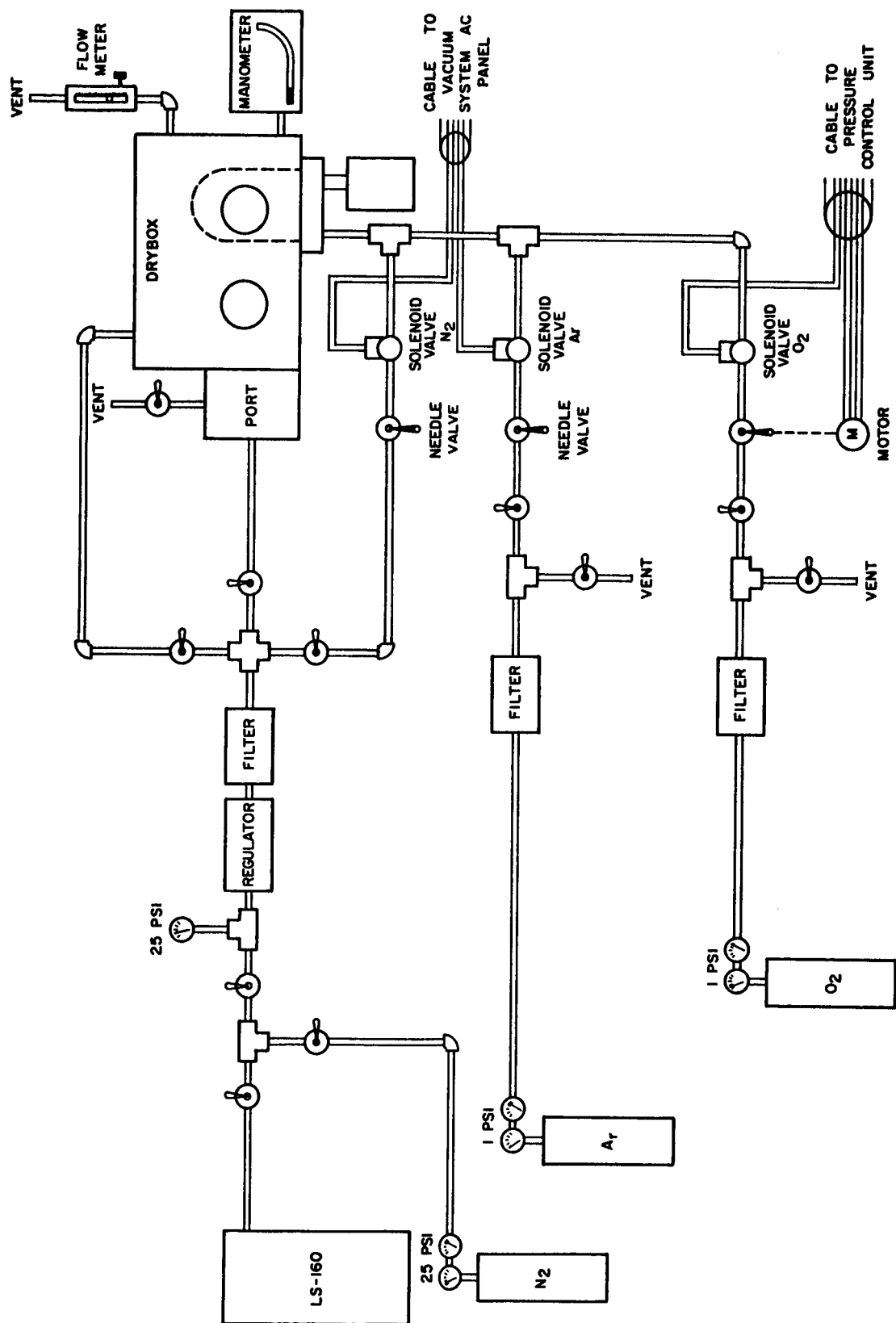


Figure A-2. Gas Feed for Vacuum System and Drybox

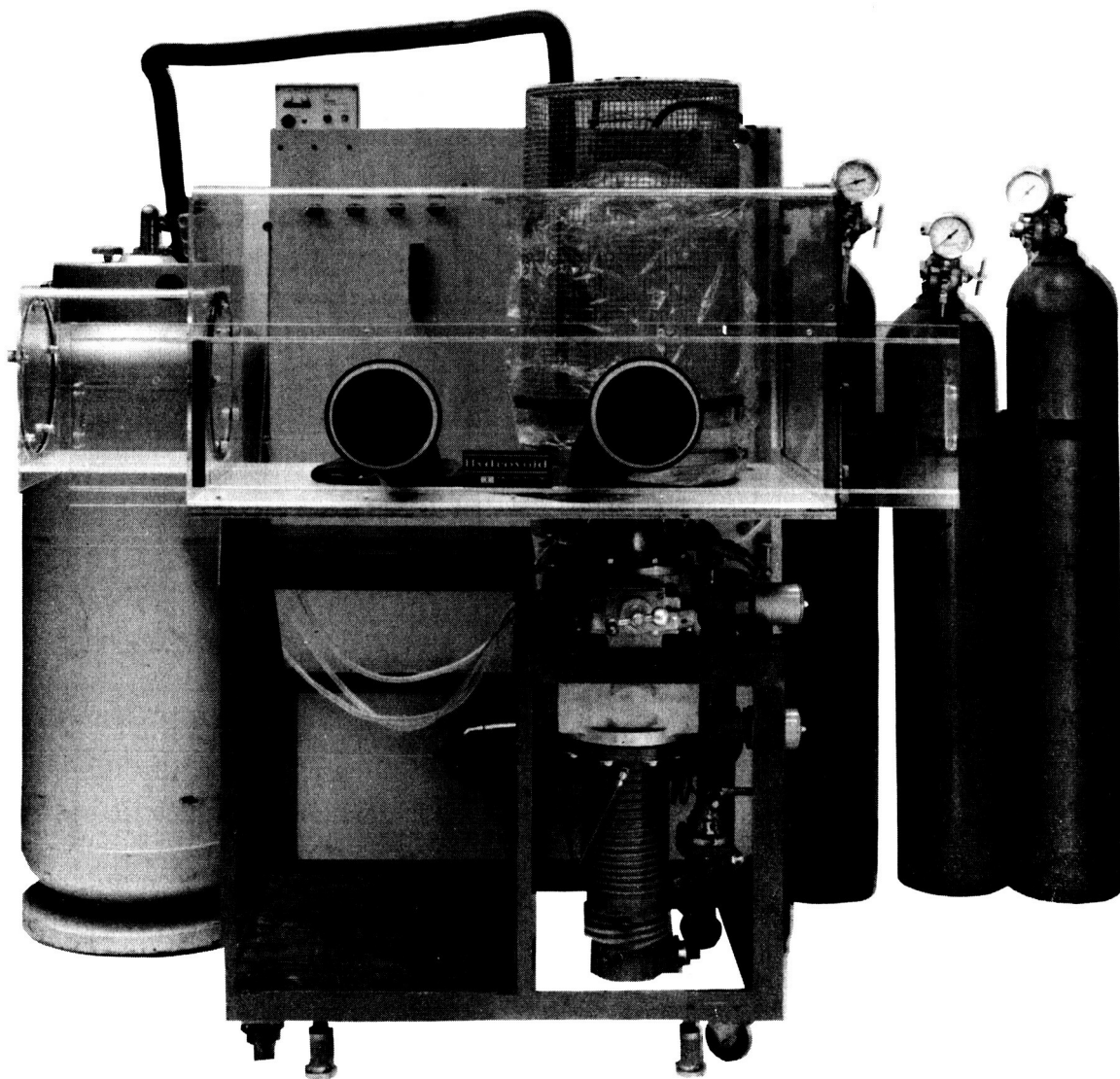


Figure A-3. Vacuum System and Drybox

APPENDIX B

PRESSURE MONITOR AND OXYGEN-PRESSURE CONTROL SYSTEM

The Pressure Monitor

A Veeco ionization gauge (RG-31-X), covering the pressure range from 10^{-3} to 10^{-11} mm mercury, is the basic pressure-sensing element. This unit also provides a recorder output of 0 to -2 volts, which is proportional to the pressure being measured.

Two Veeco thermocouple gauges, one on the roughing line and one on the backing line, provide pressure indication in the range from 1 to 1000 microns.

A Leeds and Northrup model H strip-chart recorder is connected through an attenuator to the recorder network of the ionization-gauge unit and provides continuous records of system pressure.

Pressure Controller

The pressure controller utilizes the recorder output of the pressure-gauge unit. The output voltage is attenuated and compared to a reference voltage. The resulting error voltage is amplified in a Honeywell type 356413-3 60-cycle servo amplifier which then drives a servo motor. The servo motor is coupled to a leak-valve unit mounted on the vacuum-system baseplate. Any error in pressure produces an increase or decrease in the leak-valve setting and thereby holds the pressure at the established level. A block diagram of the pressure-control system is shown in Figure B-1, and a detailed schematic diagram is shown in Figure B-2. A parts list for the pressure controller is on the page following Figure B-2. Figure B-3 is a photograph of the complete control chassis.

The leak-valve unit utilizes a Nupro needle valve driven by a Borg servo motor. Detailed drawings of this unit are shown in Figures B-4, B-5, and B-6; Figure B-7 is a photo of the assembled valve. The parts list for the servo-driven leak valve follows Figure B-4.

The pressure monitor and pressure controller are installed in a standard 6-foot relay rack which is located adjacent to the vacuum system. Figure B-8 is a photograph of the assembled unit.

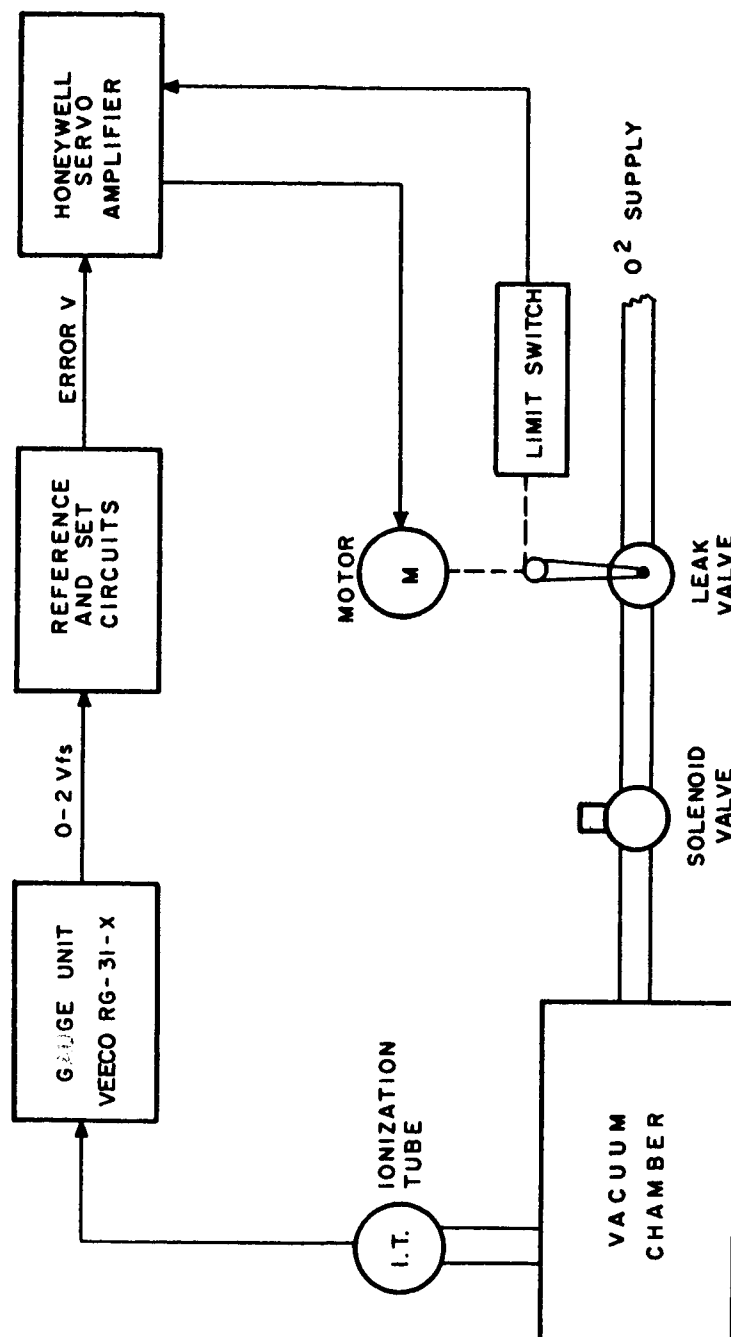


Figure B-1. Pressure-Control System, Block Diagram

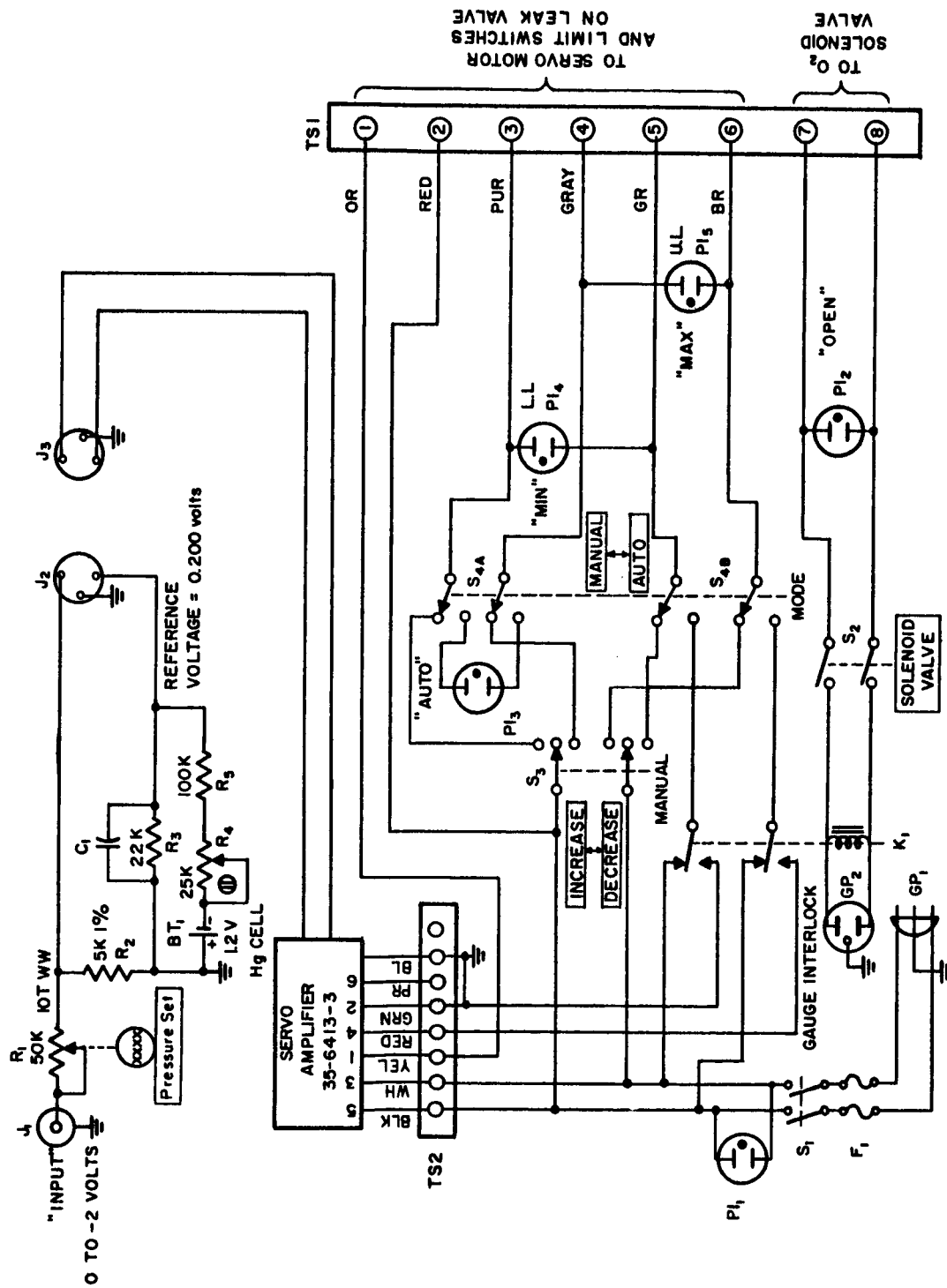


Figure B-2. Pressure Controller, Schematic Diagram

Parts List for Pressure Controller
(Figure B-2)

Symbol	Description
R ₁	50K, potentiometer, 5%, 10-turn, W.W, Borg No. 2201B
R ₂	5K, 1%, film resistor, 1/2 watt
R ₃	22K, 10%, carbon resistor, 1/2 watt
R ₄	25K, potentiometer, 2 watt
R ₅	100K, 10%, 1/2 watt, carbon resistor
C ₁	Select to provide proper damping
BT ₁	1.2-volt mercury battery, Mallory No. RM-42R
SA ₁	Servo amp., Honeywell No. 356413-3
J ₁	BNC, UG-1094/U
J ₂	Connector, audio, Amphenol No. 91-854
J ₃	Connector, audio, Amphenol No. 91-856
G _{P1}	Parallel ground plug, male
G _{P2}	Parallel ground plug, female, chassis
F ₁	Fuse, 2-ampere
S ₁ , S ₂	Switch, DPST, Cutler Hammer No. 8823K5
S ₃	Switch, DPDT, Cutler Hammer No. 8837K4
S _{4A, B}	Switch, 4PDT, Cutler Hammer No. 8838K4
Pl ₁ , Pl ₂	Pilot light, Dialco 931
Pl ₃ , Pl ₄ , Pl ₅	Indicator lights, Drake No. 110-022 (Hi Brite)
TS ₁ , TS ₂	Terminal strip, Cinch-Jones, 8-terminal
K ₁	Relay, Potter Brumfield, KL11A

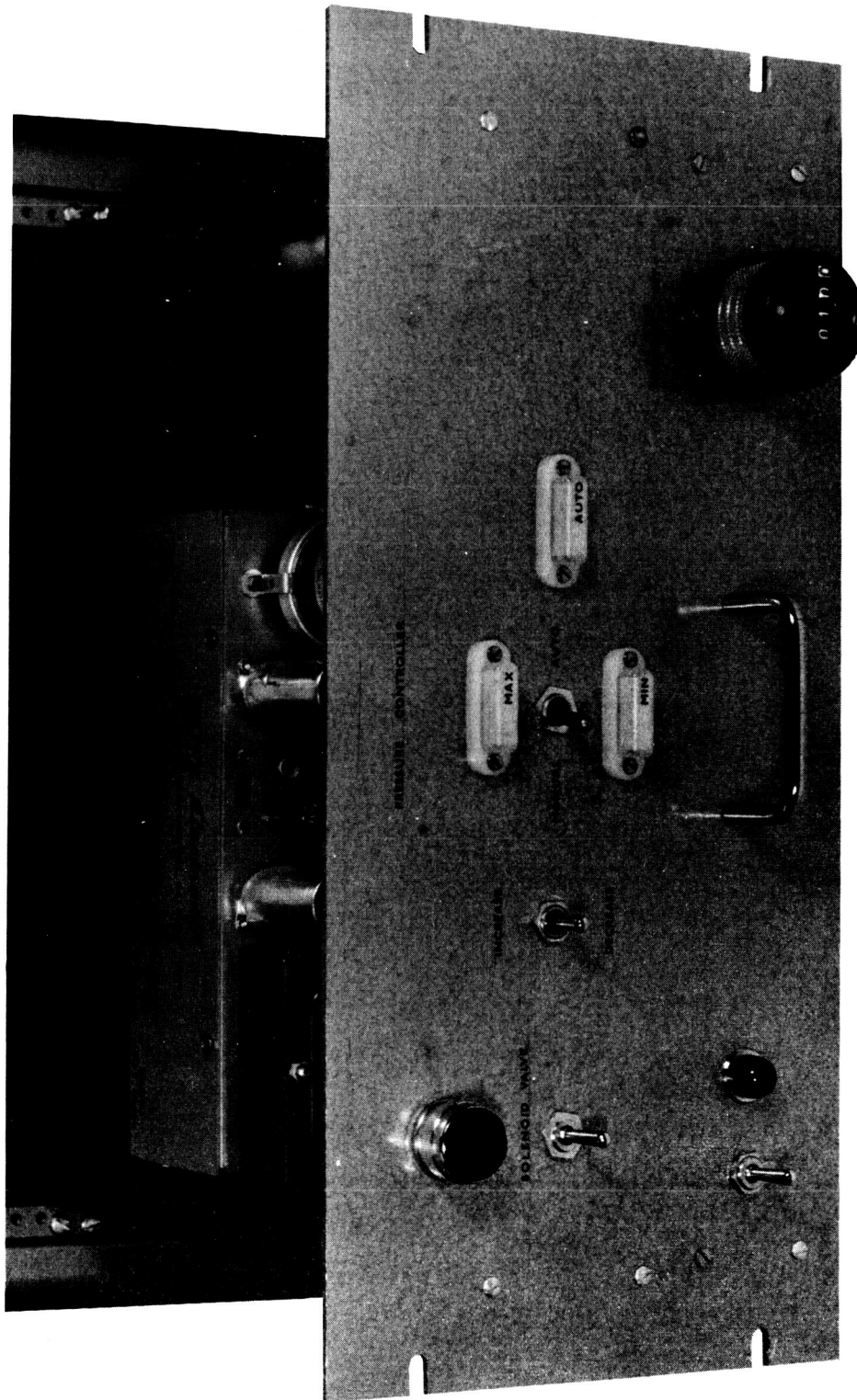


Figure B-3. Pressure Controller

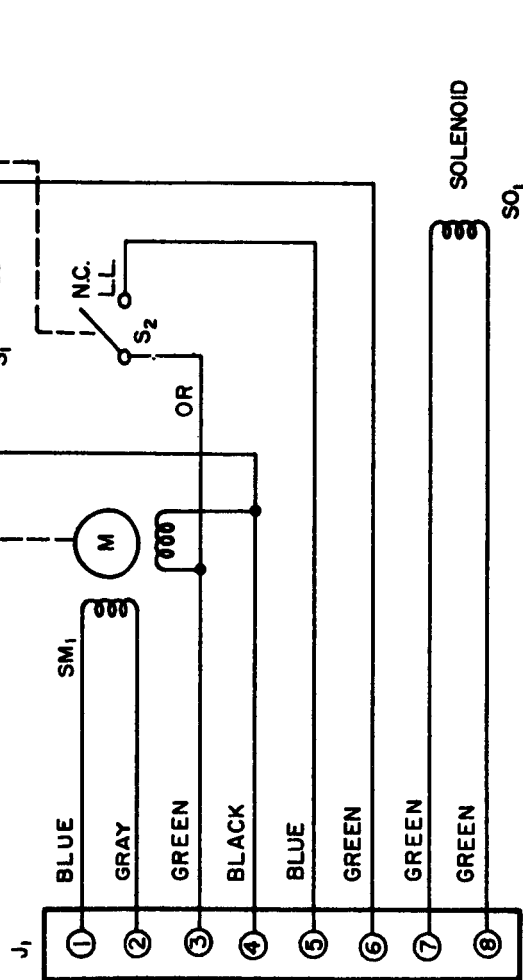


Figure B-4. Servo-Driven Leak Valve, Pressure Control System

Parts List for Servo-Driven Leak Valve
(Figure B-4)

Symbol	Description
J ₁	Female Socket, Cinch-Jones, 8-terminal S308
SM ₁	Servo motor, Borg No. 1062
S ₁	Subminiature basic switch, microswitch No. 1SX1-T (MS24547-1)
S ₂	Subminiature basic switch, microswitch No. 1SX1-T (MS24547-1)
SO ₁	Solenoid valve, Hoke B90A380G
SL ₁	Slip clutch coupling, Northfield Precision Instrument No. LCC-33
Bl ₁	Bellows coupling, Sterling No. G404-34
LV ₁	Metering valve, Nupro No. B252

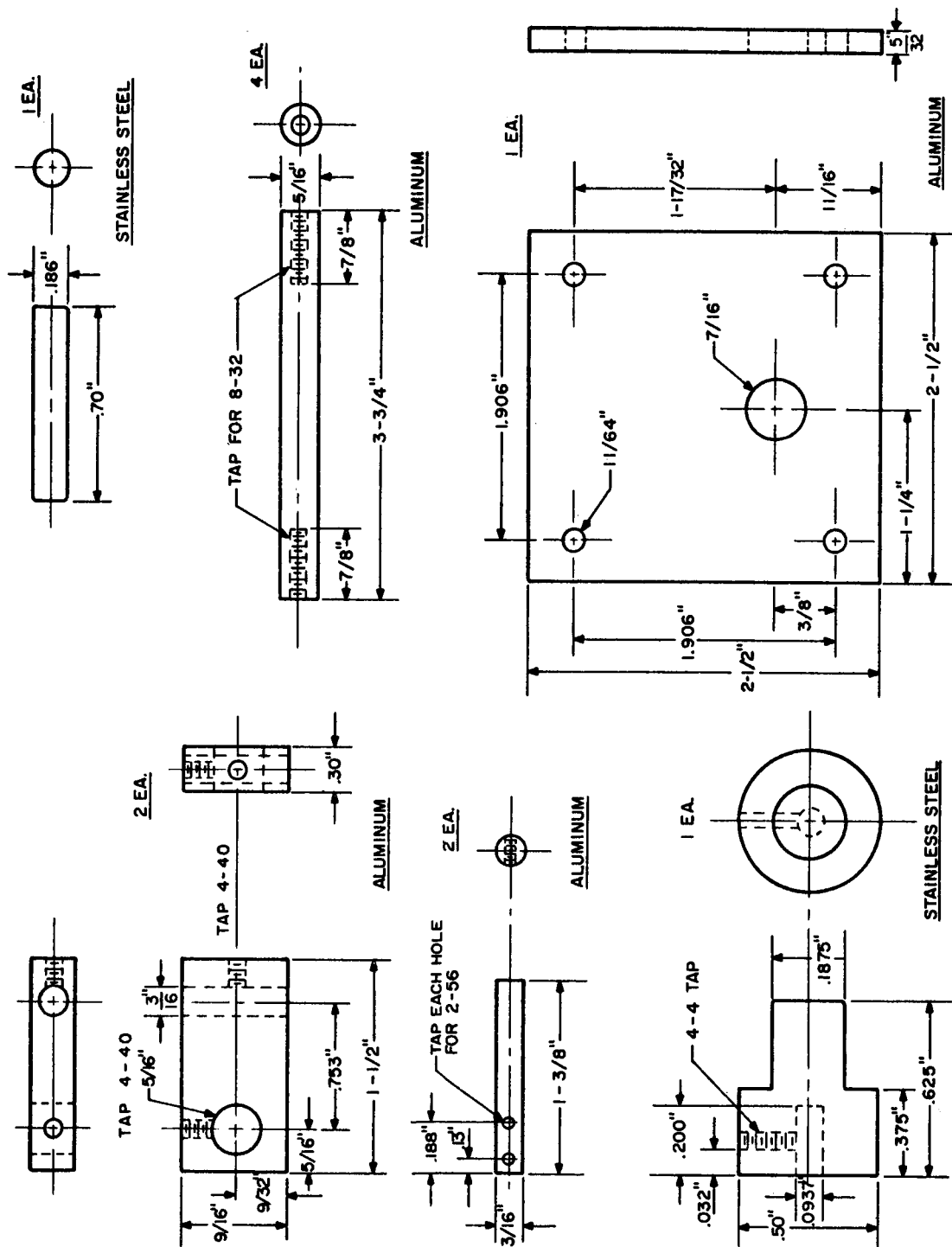


Figure B-5. Servo-Driven Leak Valve Details

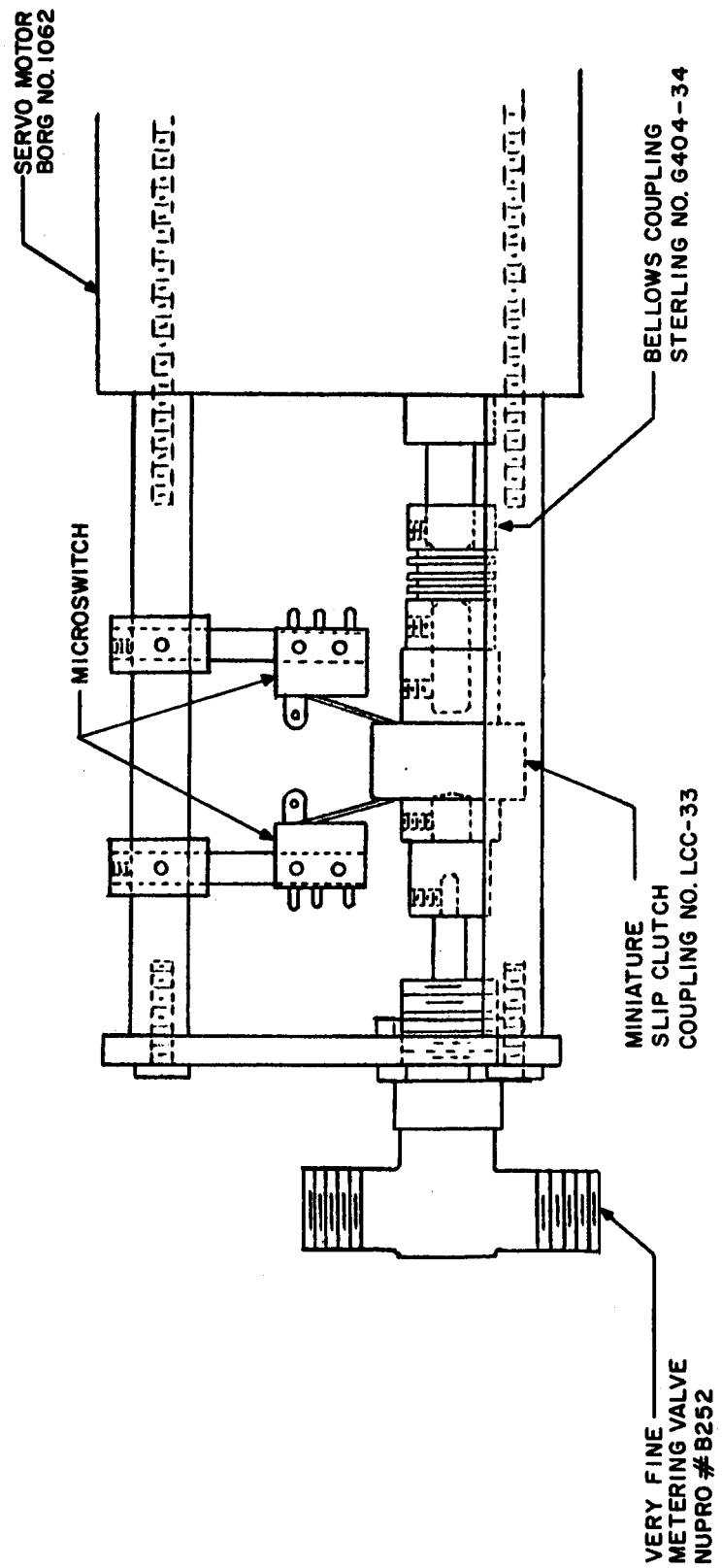


Figure B-6. Servo-Driven Leak Valve, Assembly View

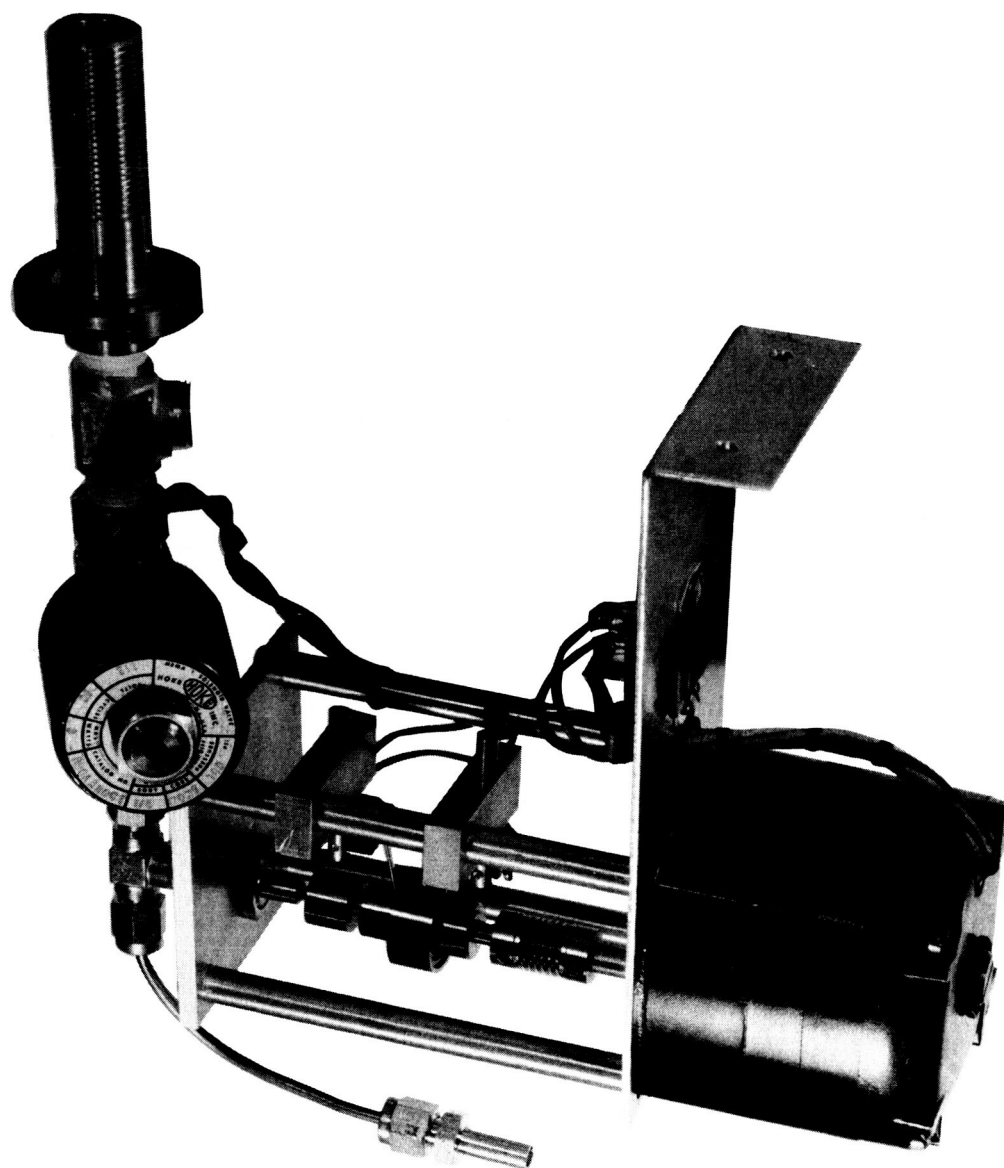


Figure B-7. Servo Leak Value

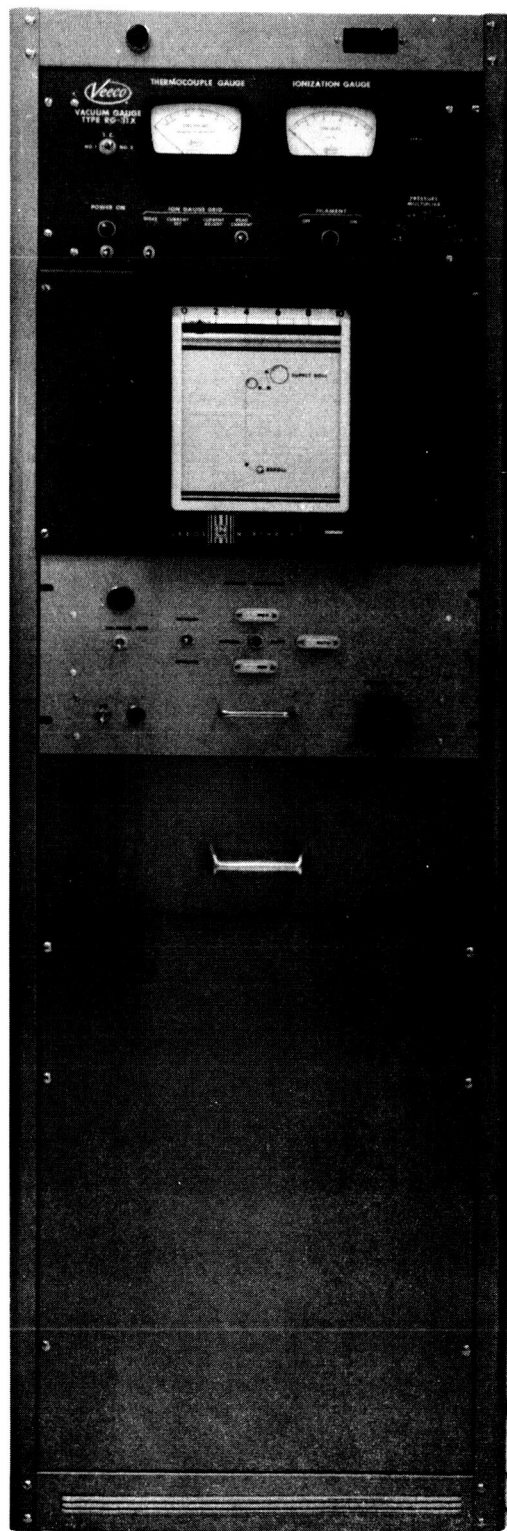


Figure B-8. Pressure Monitor and Controller

the oscillation frequency and provide a reading proportional to the frequency shift, which is the deposited mass signal. Note that the sensitivity of the R. Q. M. is a function of the normal operating frequency.

The Deposition-Control System

A block diagram of the basic deposition-control system is shown in Figure C-1. The detector unit consists of a 9.35-megacycle, crystal-controlled transistor oscillator which is placed in the vacuum system in such a location that the crystal is adjacent to the substrate and receives a characteristic sample of the material(s).

The output of the sample oscillator, a nominally 9.35-megacycle RF signal, is fed through a coaxial cable into a transistor mixer, where the difference between the sample oscillator and a reference oscillator is obtained. This difference frequency, which is typically 1 to 100 kc, is then converted by an analog frequency meter to a dc output current which is proportional to the difference frequency. As this difference frequency is proportional to deposited mass, the output of the frequency meter is proportional to the deposited mass. This signal is recorded as "Deposited Mass" on the strip-chart recorder.

An operational amplifier differentiator operates on the deposited mass signal and produces a mass deposition-rate signal, or simply, a deposition-rate signal. This voltage is recorded on the "Deposition Rate" chart recorder.

The rate signal is also fed to the rate programmer unit which consists of a variable attenuator network whose characteristics are established on the basis of the desired deposition rate. The attenuated rate signal is now compared to a reference voltage, and any difference or error signal is amplified by a servo amplifier. This resulting amplified error signal drives a servo motor which increases or decreases the voltage applied to the evaporator unit in a manner to reduce the error signal to zero and thus to correct the deposition-rate signal to the desired value.

Physical and Electrical Characteristics of Deposition-Control System

Physical features. - The complete control system is housed in a 6-foot relay rack. A frequency meter, the reference oscillator and mixer,

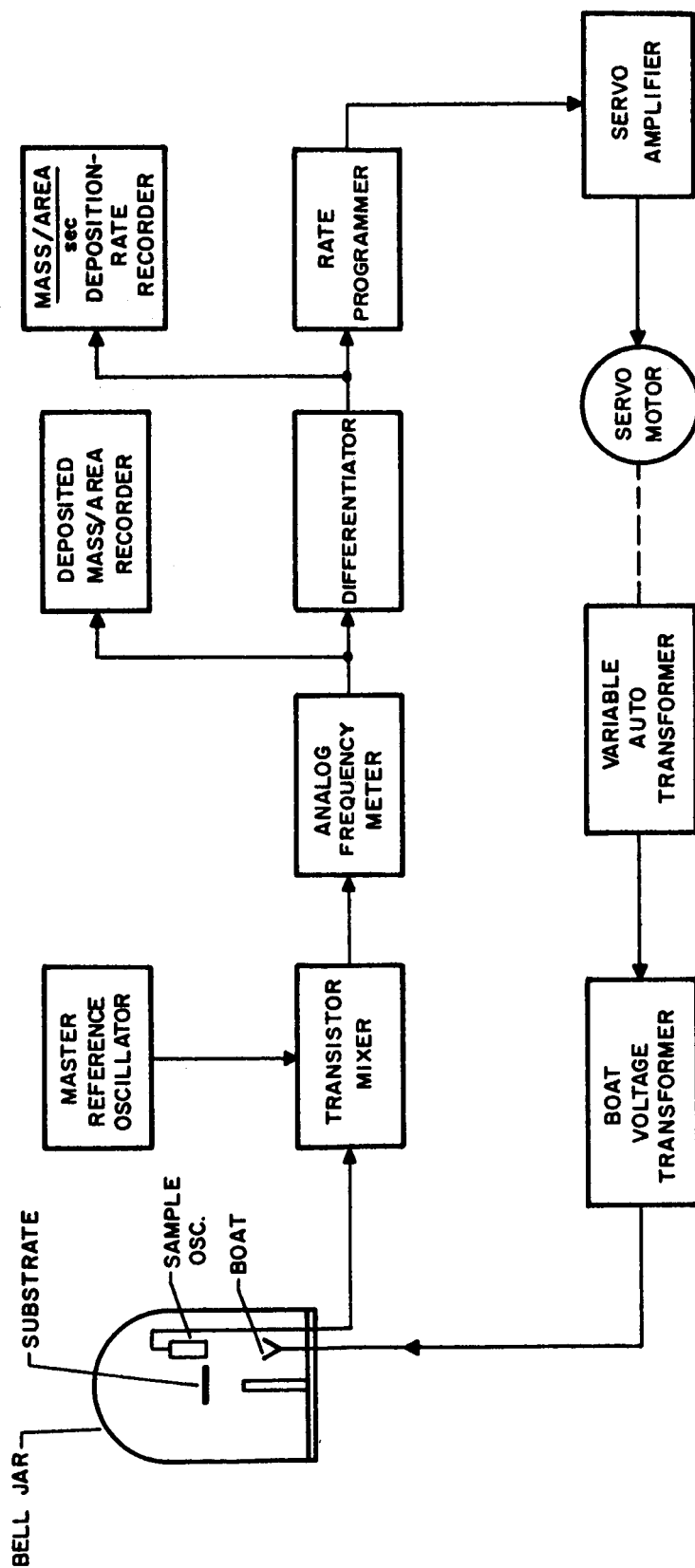


Figure C-1. R.Q.M. Deposition-Rate Controller, Block Diagram

the rate detector-programmer, the servo amplifier, and a power-control panel are mounted in the electronics rack along with the dual-channel recorder for mass and rate. Figure C-2 is a photo of the entire system less the dual-channel recorder.

Detailed description of the components. --

Sample Oscillator

The sample oscillator is a single-transistor, crystal-controlled oscillator constructed in a hermetically sealed enclosure that is installed in the vacuum system. The dc bias and ac output are handled by a single coaxial cable. Figure C-3 is a photograph of an unassembled unit, the schematic of which is shown in Figure C-4. A parts list for the sample oscillator is on the page following Figure C-4. The short-term stability of these oscillator units is better than one part in 10^7 .

A 9.350-Mc fundamental frequency was chosen to obtain the desired sensitivity. The sensitivity of the crystal resonant frequency to mass loading is given by

$$\Delta f = - \frac{f^2}{N \rho_q} \frac{M}{A} \quad 3.$$

where

Δf = frequency shift (cps)

f = fundamental frequency (9.350 Mc)

N = crystal resonant frequency coefficient (167 kc-cm)

ρ_q = mass density of quartz ($2.65 \text{ grams cm}^{-3}$)

M/A = mass per unit area of the deposit (grams cm^{-2})

Thus,

$$f = 2.00 \times 10^8 \frac{M}{A} \text{ cps}$$

and we can express the sensitivity as

$$S = 5.00 \mu\text{grams cm}^{-2} \text{ kc}^{-1}$$

3. Sauerbrey, G., op. cit.

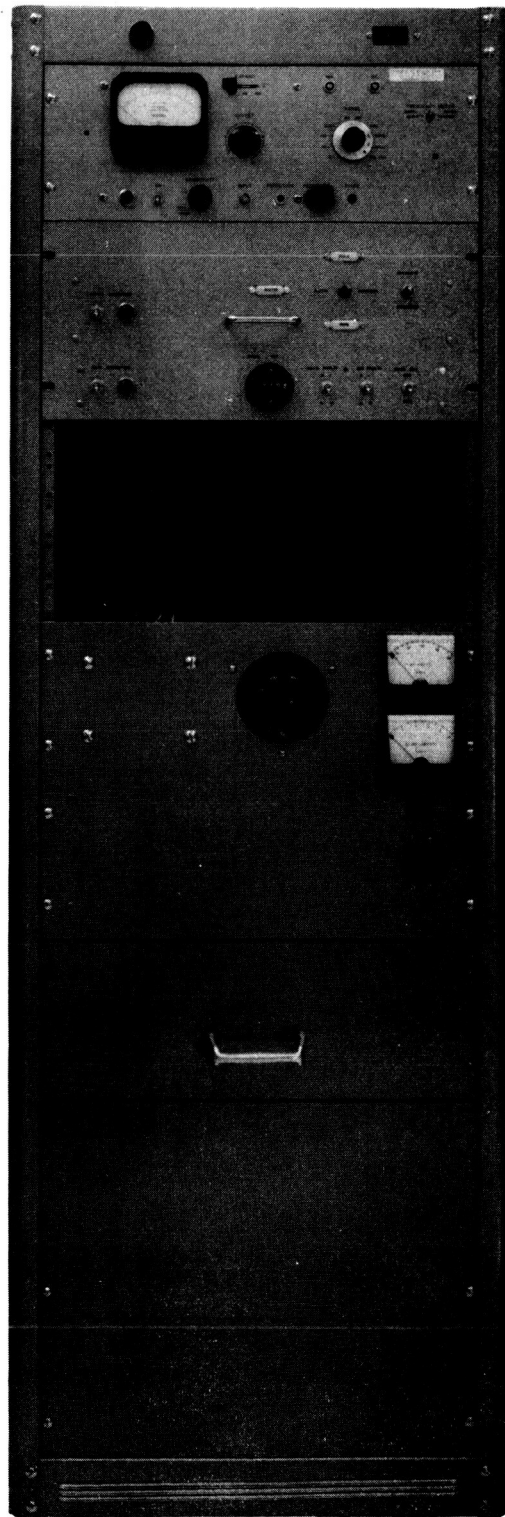


Figure C-2. Complete Control System

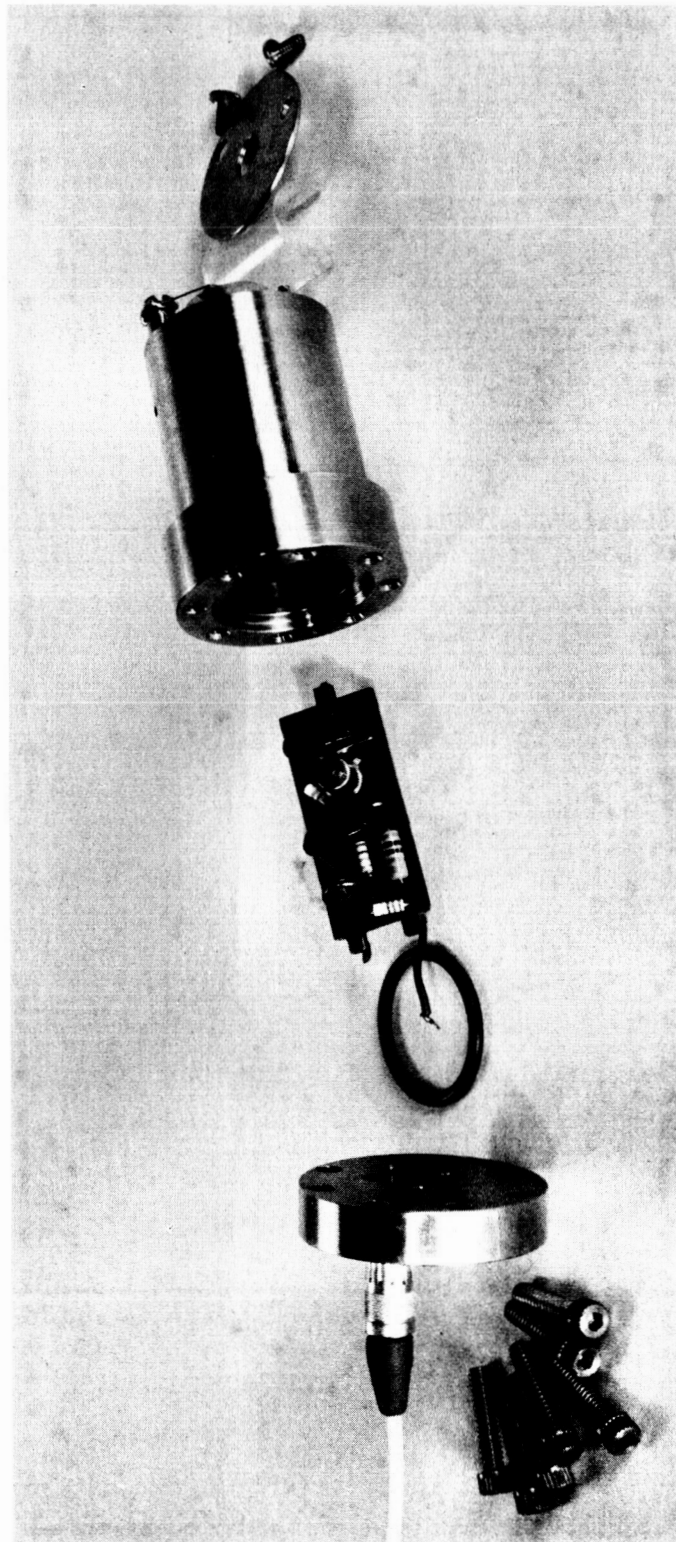
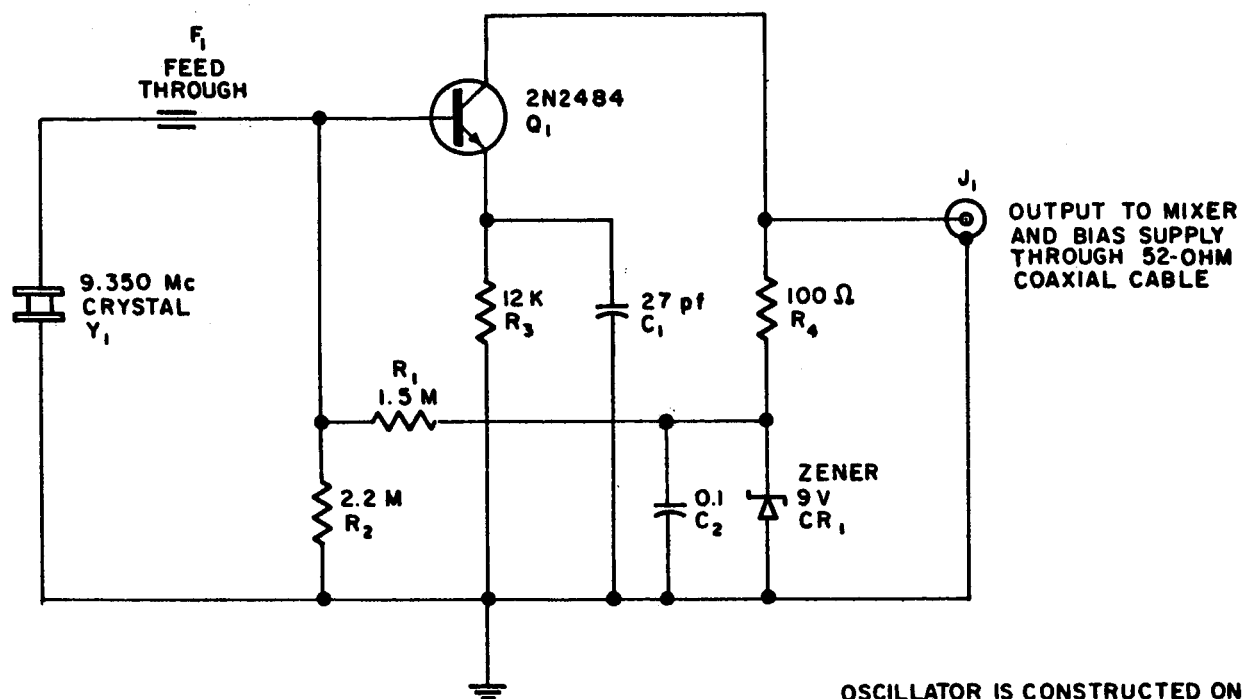


Figure C-3. Unassembled Sample Oscillator



OSCILLATOR IS CONSTRUCTED ON
AN ETCHED CIRCUIT BOARD AND
ENCLOSED IN A STAINLESS-STEEL
VACUUM-TIGHT HOUSING.

Figure C-4. Sample Oscillator, Schematic Diagram

Parts List for Sample Oscillator
(Figure C-4)

Symbol	Description
R ₁	1.5 meg., 10%, 1/10 watt, carbon resistor,
R ₂	2.2 meg., 10%, 1/10 watt, carbon resistor
R ₃	12K, 10%, 1/10 watt, carbon resistor
R ₄	100 ohm, 10%, 1/10 watt, carbon resistor
C ₁	27 pf, mica capacitor
C ₂	0.01 μ f, 25 vdcw, disc capacitor
Q ₁	Transistor, 2N2484
CR ₁	Zener diode, 1N713
Y ₁	9.350-Mc crystal, 0.005%, series resonant, Bliley No. BH6A
J ₁	Microdot slide-on receptacle, No. 51-158
F ₁	Feed through, ceramic, No. 800A0720-1 Ceramaseal, Inc.

Figure C-5 is the circuit-board layout for the sample oscillator. The mechanical details of the oscillator housing are covered in Figures C-6, C-7, and C-8, and a completed assembly view is shown in Figure C-9.

The quartz crystal is mounted on the face end of the sample oscillator housing with two wire clips. Figure C-10 is a photograph of the oscillator unit with a crystal installed but with the crystal mask removed.

Reference oscillator and mixer

A transistorized master reference oscillator, buffer amplifier, and transistor mixer are located on a subchassis in the deposition-rate monitoring unit. A schematic of this subchassis is shown in Figure C-11; the parts list for Figure C-11 appears on the page following the schematic.

Analog frequency meter

A Hewlett-Packard 500 BR frequency meter provides the conversion from a difference-frequency signal to a dc current. The frequency-meter unit has been modified in the following way:

- a. A hum-bucking network, consisting of a series resistance and capacitance, was connected from the secondary of the high-voltage transformer to ground. The component values are adjusted to minimize the residual 60 cps in the recorder output.
- b. The gas reference tube in the power supply has been replaced by a semiconductor diode to improve the stability of the power supply.
- c. The 6AL5 phototube bias rectifier was removed.

The net result of these changes is to reduce the 60-cycle hum in the output signal and to improve the stability. In addition, rear-mounted input and output connections are installed.

The frequency-meter output is always 1.0 ma for a full-scale reading; thus,

$$I_f = \frac{f_f}{f_o} \times I_o \text{ amps}$$

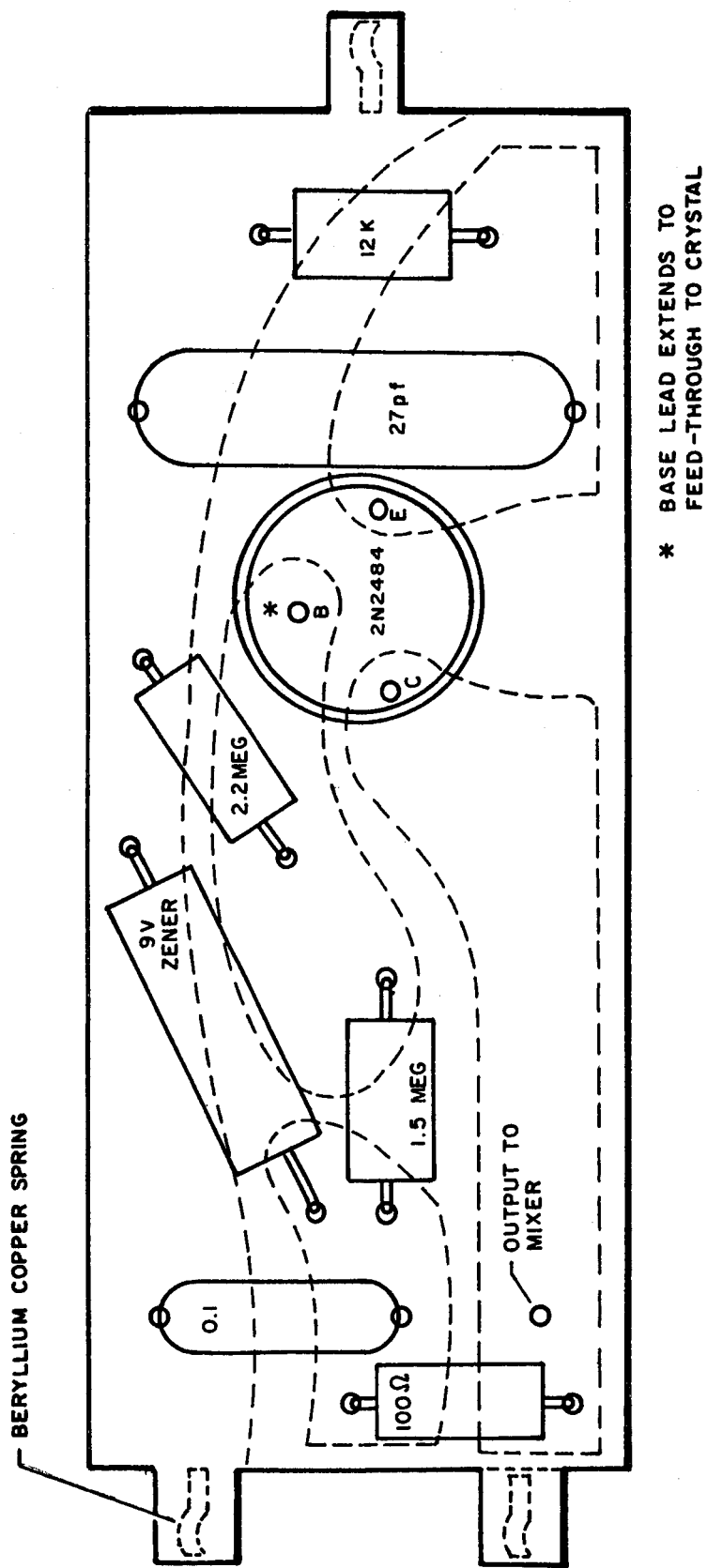
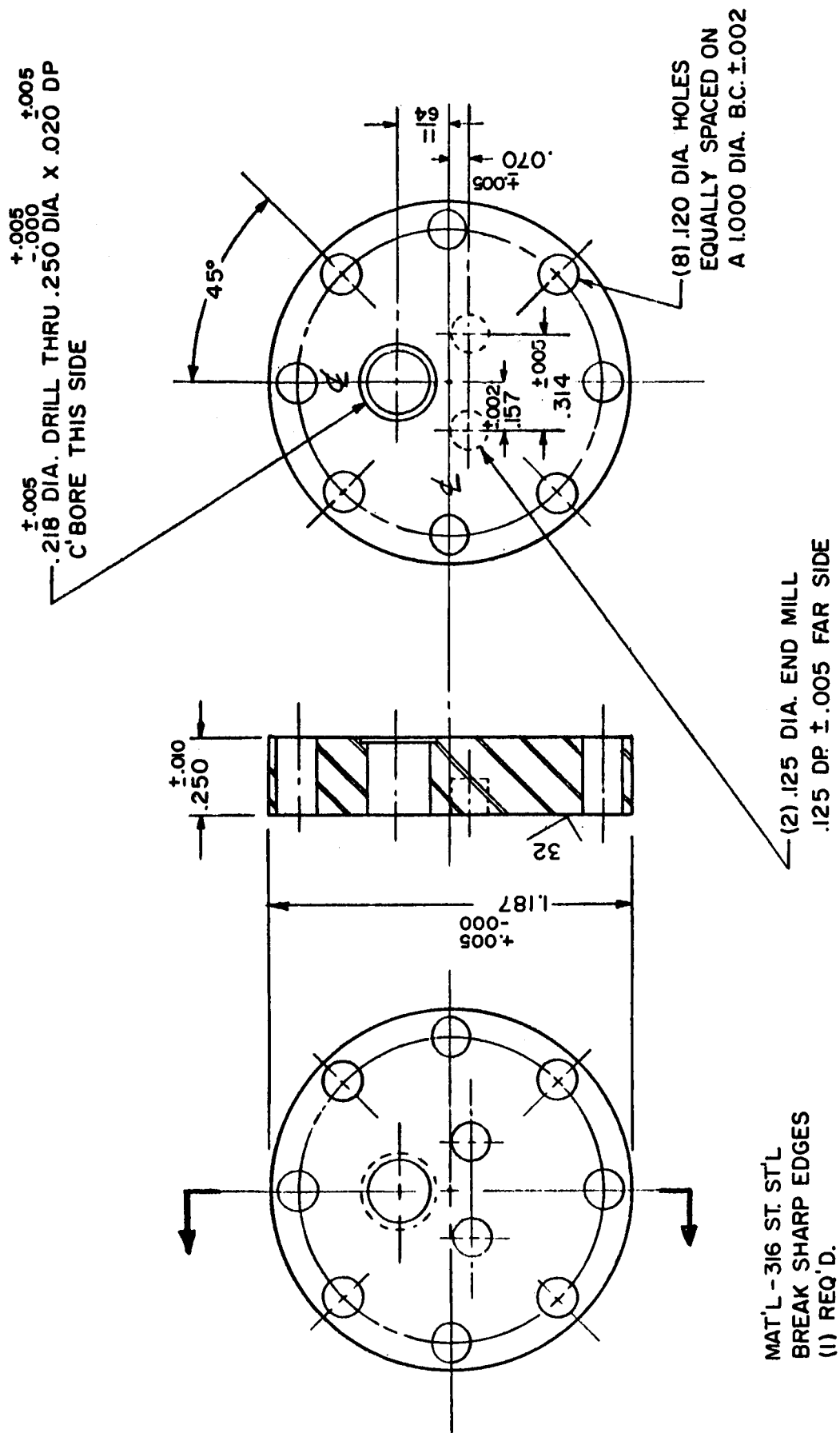


Figure C-5. Circuit Board for Quartz Crystal Microscale Sample Oscillator



MAT'L - 316 ST. ST'L
BREAK SHARP EDGES
(1) REQ'D.

Figure C-7. End Plate

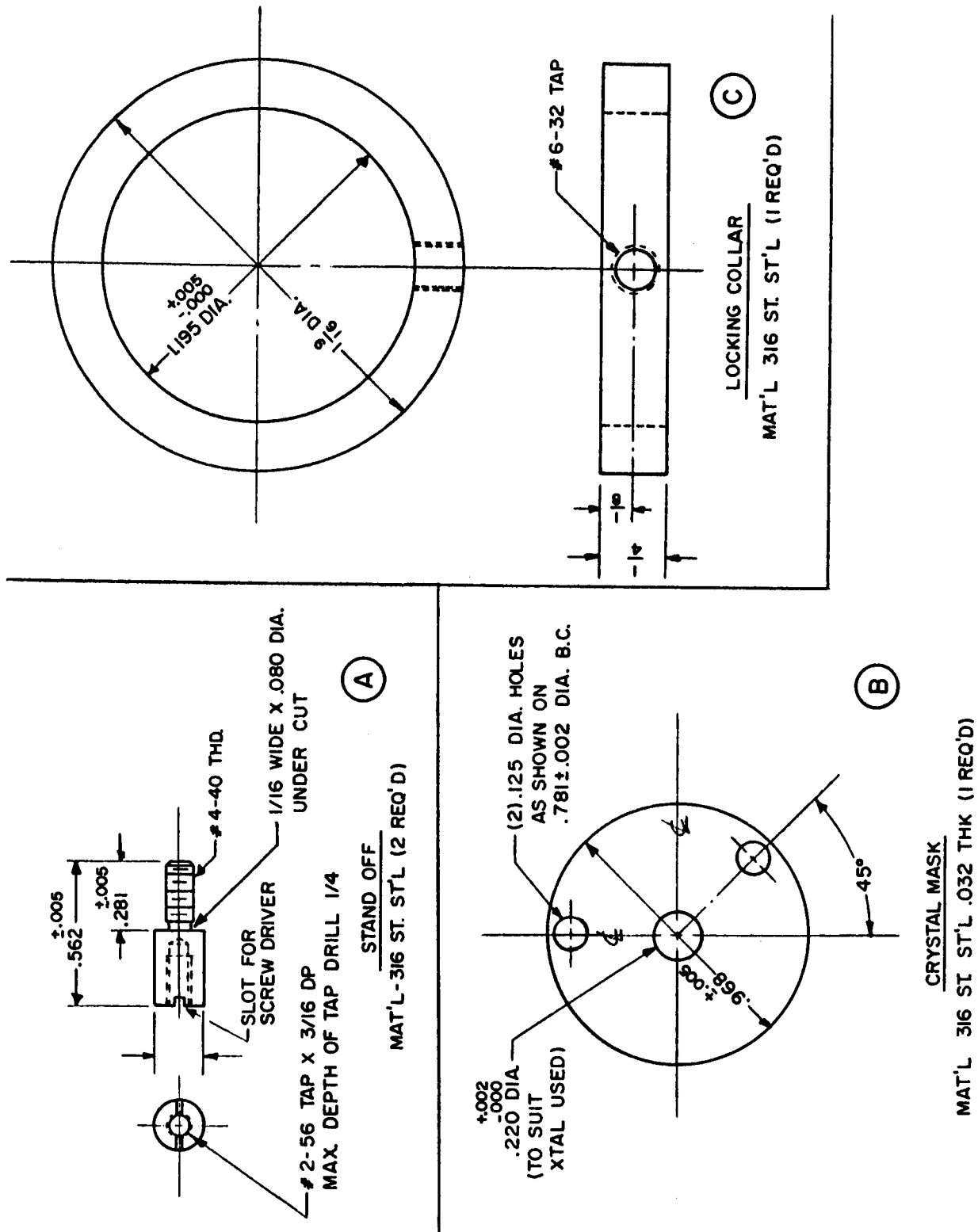


Figure C-8. Details

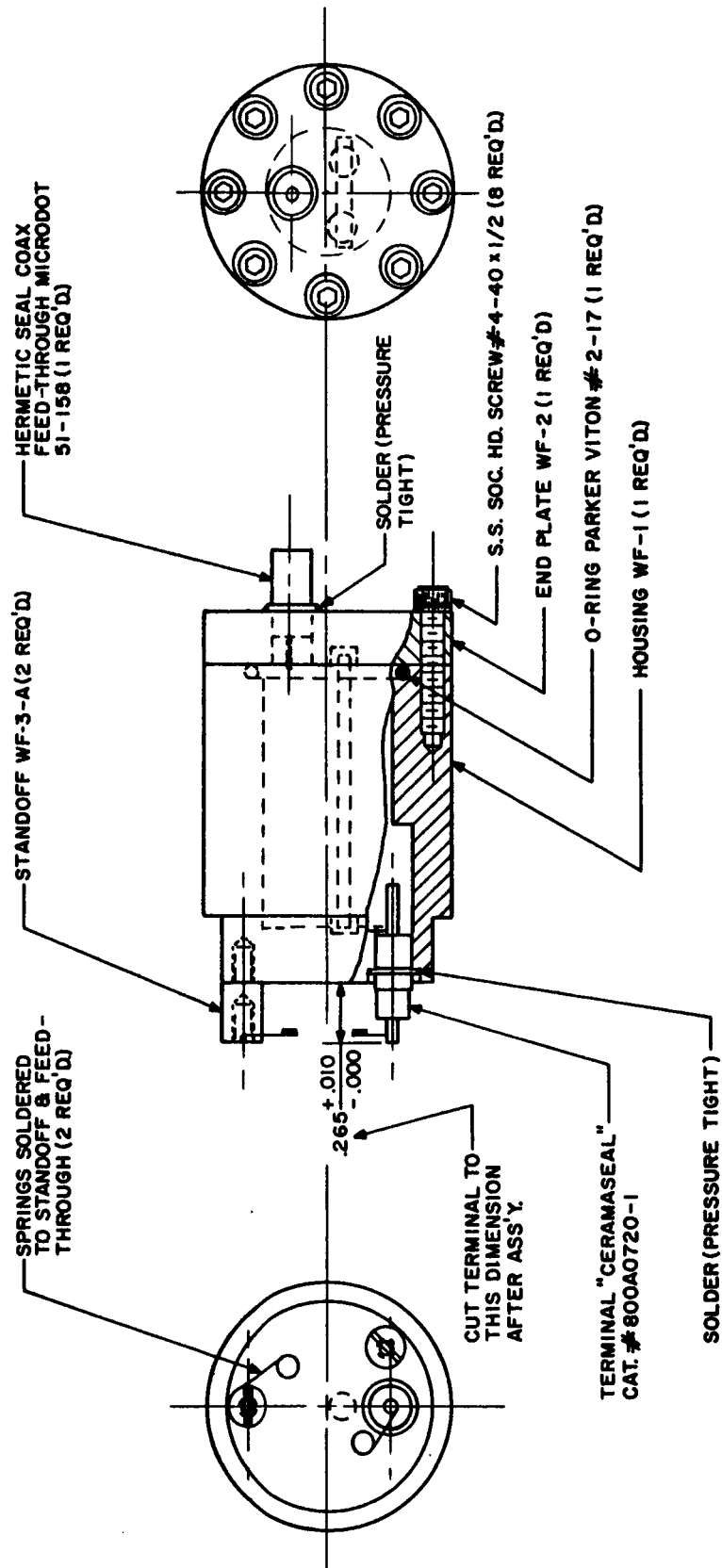
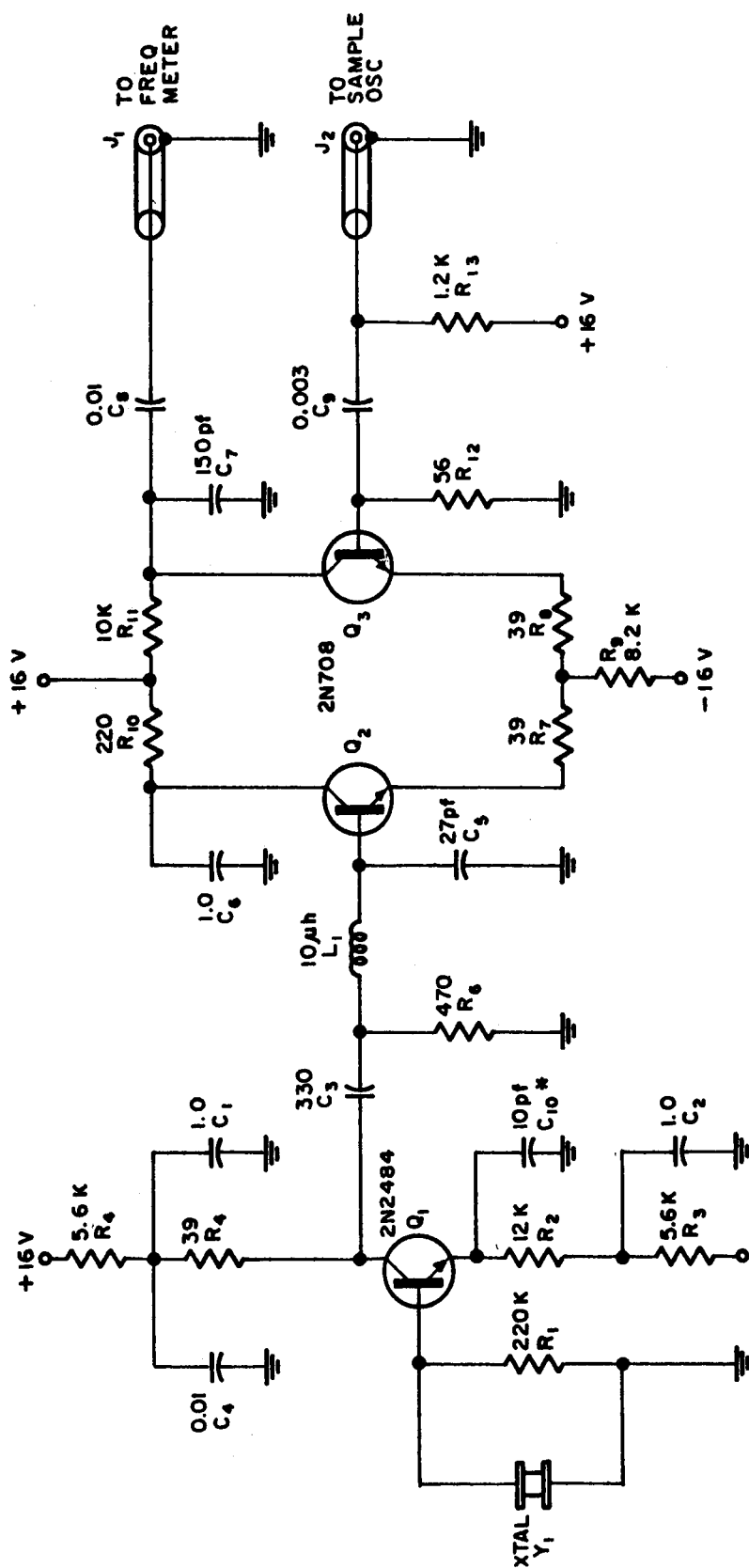


Figure C-9. Ultrahigh-Vacuum Crystal Oscillator



Figure C-10. Assembled Sample Oscillator



* SELECT FOR PROPER
REFERENCE FREQUENCY

Figure C-11. Master Reference Oscillator and Mixer

Parts List for Master Reference Oscillator and Mixer
(Figure C-11)

Symbol	Description
R ₁	220K, 10%, 1/2 watt, carbon resistor
R ₂	12K, 10%, 1/2 watt, carbon resistor
R ₃ , R ₅	5.6K, 10%, 1/2 watt, carbon resistor
R ₄ , R ₇ , R ₈	39 ohms, 10%, 1/2 watt, carbon resistor
R ₆	470 ohms, 10%, 1/2 watt, carbon resistor
R ₉	8.2K, 10%, 1/2 watt, carbon resistor
R ₁₀	220 ohms, 10%, 1/2 watt, carbon resistor
R ₁₁	10K, 10%, 1/2 watt, carbon resistor
R ₁₂	56 ohms, 10%, 1/2 watt, carbon resistor
R ₁₃	1.2K, 10%, 1/2 watt, carbon resistor
C ₁ , C ₂ , C ₆	1.0 μ f, disc capacitor, 25 vdcw
C ₃	330 pf, mica capacitor
C ₄ , C ₈	0.01 μ f disc capacitor, 25 vdcw
C ₅	27 pf, mica capacitor
C ₇	150 pf, mica capacitor
C ₉	0.003 μ f disc capacitor, 25 vdcw
C ₁₀ [*]	10 pf, mica capacitor

* Select for proper reference frequency.

Parts List for Master Reference Oscillator and Mixer (Cont)
(Figure C-11)

Symbol	Description
Q_1	Transistor, 2N2484
Q_2, Q_3	Transistor, 2N708
Y_1	9.350-Mc crystal, 0.005%, series resonant, Bliley No. BC61A
L_1	10 μ h, molded RF choke
J_1, J_2	BNC, UG-1094/U

where

f_o is full-scale reading

f_f is frequency-meter reading

I_o is 1 ma.

The frequency shift is proportional to the mass deposit

$$\Delta f = \frac{\sigma}{S}$$

where

σ is surface mass in $\mu\text{grams cm}^{-2}$

S is sensitivity in $\mu\text{grams cm}^{-2} \text{ cycle}^{-1}$

In using this system, one can neglect any initial frequency-meter reading as being equivalent to a previous deposited mass;

$$\therefore f_f = \frac{\sigma}{S}$$

where

f_f = frequency-meter reading.

$$I_f = \frac{f_f}{f_o} I_o \text{ from frequency meter}$$

$$I_f = \frac{\sigma}{S} \frac{I_o}{f_o}$$

Mass recorder

The mass recorder voltage is obtained from the voltage drop across R_3 , Figure C-12; the parts list for Figure C-12 appears on the page following the schematic.

Figure C-12. Rate Detector

Parts List for Rate Detector
(Figure C-12)

Symbol	Description
R ₁	400 ohms, 1%, film resistor, 1/2 watt
R ₂	990 ohms, 0.1%, film resistor, 1/2 watt
R ₃	10 ohms, 0.1%, film resistor, 1/2 watt
R ₄	56K, 1%, film resistor, 1/2 watt
R ₅	4.7 meg., 1%, film resistor, 1/2 watt
R ₆	470K, 1%, film resistor, 1/2 watt
R ₇	100K, potentiometer, carbon, 2-watt
R ₈	1 meg., potentiometer, carbon, 2-watt
R ₉	2.5K, 0.1%, film resistor, 1/2 watt
R ₁₀	50K, 5%, potentiometer, 10-turn W.W., Borg No. 2201B
R ₁₁	4.5K, 0.1%, film resistor, 1/2 watt
R ₁₂	500 ohms, 0.1%, film resistor, 1/2 watt
R ₁₃	100 ohms, potentiometer, carbon, 2 watt
R ₁₄	150 ohms, 1%, film resistor, 1/2 watt
R ₁₅	270K, 1%, film resistor, 1/2 watt
R ₁₆	27K, 1%, film resistor, 1/2 watt
R ₁₇	320K, 1%, film resistor, 1/2 watt
C ₁ , C ₂ , C ₃	105 μ f 15 vdc, tantalum, electrolytic, Sprague No. 107X901OR2
C ₄	1.0 μ f 200 vdc, molded paper capacitor

Parts List for Rate Detector (Cont)
(Figure C-12)

Symbol	Description
C ₅	0.1 μ f 200 vdc, molder paper capacitor
C ₆	Selected to provide proper damping; typically 50-100 μ f electrolytic
C ₇ , C ₈ , C ₉ , C ₁₀	0.001 μ f feed-through capacitor, Centralab No. FT
J ₁	BNC UG-1094/U
J ₂ , J ₃ , J ₄	Connector, audio, female, Amphenol No. 91-856
D ₁ , D ₂	Diode, FD100
S ₁ , S ₃ , S ₄	Switch, SPDT, Cutler-Hammer No. 8836K4
S ₂	Switch, DPDT, Cutler-Hammer No. 8837K4
P ₂	Differential operational amplifier, Philbrick Research, Inc., P2A
F ₁	Fuse, 2 ampere
G _{p1}	Parallel ground plug, male
Pl ₁	Pilot light, Dialco No. 931
QM ₁ , QM ₂	Power supply, 16v, 100 ma, Technipower No. M-158-0.100

Thus, mass recorder voltage

$$V_{\sigma} = I_f R_3 = \frac{\sigma}{S} \frac{I_o}{f_o} R_3$$

$$I_o = 10^{-3} \text{ amps}$$

$$S = 5 \text{ } \mu\text{grams cm}^{-2} \text{ kc}^{-1}$$

$$R = 10 \text{ ohms}$$

$$f_o = \text{frequency-meter setting in cycles}$$

$$V_{\sigma} = \sigma \left[\frac{10^3}{f_o} \times \frac{10^{-3} \times 10}{5 \times} \right] = \sigma \frac{2}{f_o}$$

or

$$\sigma = \frac{V_{\sigma} f_o}{2} \text{ in } \mu\text{grams cm}^{-2}$$

The differentiator or rate detector

The differentiator circuit shown in Figure C-12 uses an operational amplifier to obtain stable, low-noise differentiation of the mass versus time signal, and provides a low-impedance output to drive the rate recorder and the rate programmer network. The circuit is a variation of the one suggested by the G. A. Philbrick Company. The output of the differentiator is a dc voltage that is proportional to the rate of change of the deposited mass signal and which is proportional to the deposition rate. A deposition-rate multiplier is included as part of the differentiator. This range switching is achieved by varying the feedback resistor. The rate multiplication factor is 10 to 1. The capability of changing the sensitivity of the differentiator in this manner increases the versatility of the deposition control system by allowing one to choose the optimum frequency-meter setting for the desired deposited mass and still obtain optimum rate-detector performance. The output of the rate detector (differentiator) is fed directly to the deposition recorder. The magnitude of this signal is proportional to the deposition

rate and may range from 0 to 100 millivolts. The actual calibration of this signal is dependent upon the frequency-meter settings and the differentiator multiplier setting.

The following are differentiator circuit equations (ref. Figure C-12):

The differentiator output is

$$e_d = \frac{dV_{in}}{dt} R_f C_3$$

where

R_f is feedback resistor, either R_5 or R_6 , depending on differentiator multiplier (S_3) setting.

V_{in} is the input voltage produced by the frequency-meter current flowing through R_2 and R_3

$$V_{in} = I_f (R_2 + R_3)$$

$$\frac{dV_{in}}{dt} = \frac{d I_f}{dt} (R_2 + R_3)$$

Therefore,

$$e_d = \frac{d I_f}{dt} (R_2 + R_3) R_f C_3$$

as before

$$I_f = \frac{\sigma}{S} \frac{I_o}{f_o}$$

as only σ is time variant

$$\frac{d I_f}{dt} = \frac{d \sigma}{dt} \frac{I_o}{S f_o}$$

$$\frac{d \sigma}{dt} \text{ is deposition rate } (\mu\text{gams cm}^{-2} \text{ sec}^{-1})$$

define

$$\frac{d\sigma}{dt} \quad D \equiv \mu\text{grams cm}^{-2} \text{ sec}^{-1}$$

$$\frac{dI_f}{dt} = D \frac{I_o}{Sf_o}$$

Therefore,

$$e_d = D \frac{I_o}{Sf_o} (R_2 + R_3) R_f C_3$$

Substituting

$$I_o = 10^{-3} \text{ amps full scale}$$

$$S = 5 \mu\text{grams cm}^{-2} \text{ kc}^{-1}$$

$$R_2 = 990 \text{ ohms}$$

$$R_3 = 10 \text{ ohms}$$

$$C_3 = 105 \mu\text{f nominal}$$

$$R_{f1} = R_5 + R_8 = 4.76 \times 10^6 \text{ ohms nominal} \quad \times 1 \text{ on Diff. Mult.}$$

or

$$R_{f10} = R_6 + R_7 = 4.76 \times 10^5 \text{ ohms nominal} \quad \times 10 \text{ on Diff. Mult.}$$

$$\text{In calibration } \frac{R_{f1}}{R_{f10}} = 10/1 \quad \text{and}$$

R_{f1} and R_{f2} are adjusted to produce the desired calibration allowing for the variation in C_3 ($R_{f1} C_3 = 500 \text{ sec}$).

Therefore,

$$e_d = \frac{D \cdot 10^{-3}}{f_o \cdot 5 \cdot 10^{-3}} \left(1,000 \left(\frac{4.76 \times 10^{-6}}{M_D} \right) (10^5) (10^{-6}) \right)$$

where M_D is setting of S_3 , 1 or 10

$$e_d = \frac{D \cdot 5 \times 10^5}{f_o \cdot 5 \cdot M_D} \text{ volts } \mu\text{grams}^{-1} \text{ cm}^{-2} \text{ sec}^{-1}$$

$$e_d = \frac{D}{f_o \cdot M_D} \times 10^5$$

or

$$D = e_d \frac{f_o \cdot M_D}{10^5} \mu\text{grams cm}^{-2} \text{ sec}^{-1}$$

Rate recorder

The output (e_d) of the differentiator is fed directly to the rate recorder. Thus, the deposition rate can be read directly from the recorder as

$$D = e_d \left[\frac{f_o \cdot M_D}{10^5} \right] \mu\text{grams cm}^{-2} \text{ sec}^{-1}$$

Rate programmer unit

The rate programming unit provides the means for achieving the desired deposition rate. Fundamentally, the rate programmer is a simple resistive divider. The input voltage to this divider is proportional to the deposition rate. The output voltage, a fraction of the input voltage, is compared to a reference voltage by the servo amplifier and held constant. This produces a transfer function as shown below (cf. Figure C-13).

e_r = output voltage = reference voltage = a constant

e_d = deposition-rate signal from differnetiator

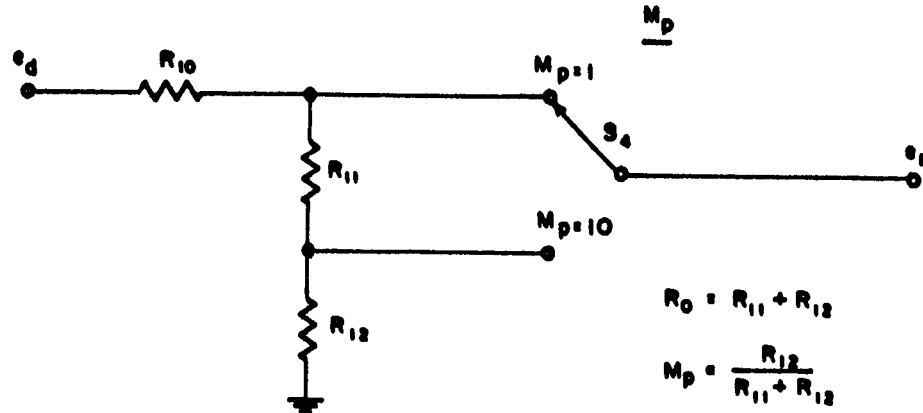


Figure C-13. Rate Programmer Network

For this network let

$$N = \left(1 + \frac{R_1}{R_0} \right) ; \text{ therefore, } \frac{e_d}{e_r} = M_p N$$

R_{10} can now be changed to provide a linear variation of the deposition rate if

$$R_{10\max} = 10 R_0$$

and

$$R_{10} = R_{10\max} X, \quad 0 \leq X \leq 1$$

Then,

$$N = 1 + \frac{X R_{10\max}}{R_o} = 1 + X \frac{10R_o}{R_o} = 1 + 10X$$

If R_{10} is fitted with a dial which reads 1.0 when $R = 0$ ($X = 0$) and 11 for $R_{10} = R_{10\max}$ ($X = 1$) then N is dial reading. A variation of 1.0 to 11 in N obtained with a direct-reading dial on the 10-turn rheostat used for R_{10} .

Combining the rate programmer and the differentiator equations,

$$M_p N = \frac{e_d}{e}$$

and

$$e_d = \frac{D}{f_o M_D} \times 10^5$$

$$D = \frac{N e_r f_o M_D M_p}{10^5}$$

e_r is set to 0.010 volt during calibration.

Therefore,

$$D = N f_o M_D M_p \times 10^{-7} \text{ } \mu\text{grams cm}^{-2} \text{ sec}^{-1}$$

This is the defining equation of the rate-control system.

Servo Amplifier

The servo amplifier is a Minneapolis-Honeywell unit containing a chopper for converting the dc signals to 60-cycle ac suitable for driving the servo motor. This is a standard unit with no modifications. A damping network as shown in Figure C-12 ($C_6 R_{15}$) suppresses the tendency of the servo system to oscillate. The time constant of the damping network must be adjusted to an optimum value that is dependent upon the physical construction of the evaporator unit. The wiring of the servo amplifier and its controls is shown in Figure C-14. The parts list for this unit is on the page following the illustration.

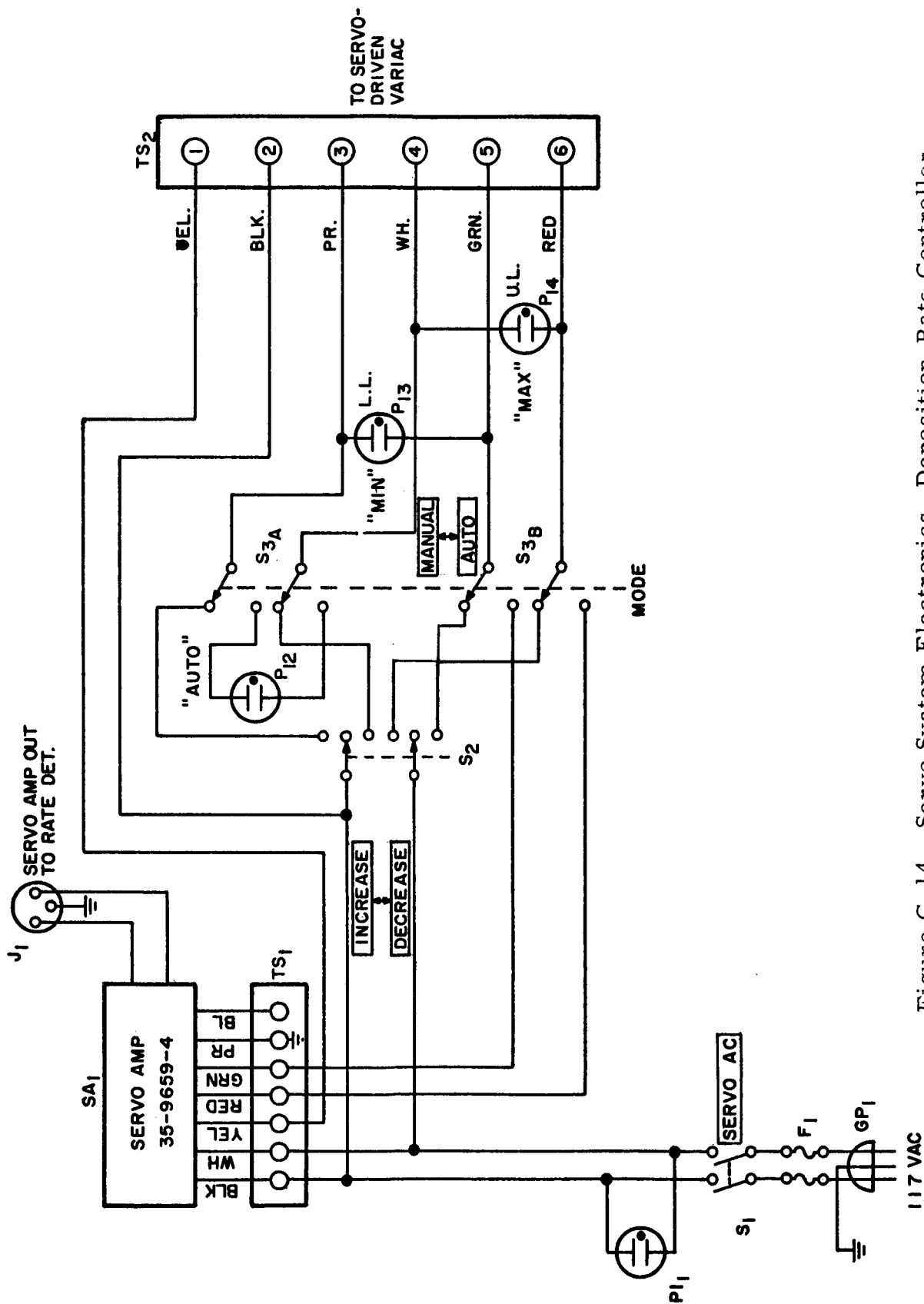


Figure C-14. Servo System Electronics, Deposition-Rate Controller

Deposition-Rate Controller Servo System
(Figure C-14)

Symbol	Description
G _{P1}	Parallel ground plug, male
F ₁	Fuse, 1 ampere, slow-blow
Pl ₁	Pilot light, Dialight No. 931
S ₁	Toggle switch, ac, Cutler-Hammer No. 8823K5
SA ₁	Servo amplifier, Honeywell No. 35-9659-4
J ₁	Connector, audio, male, Amphenol 91-853
T _{S1}	Terminal strip, Cinch-Jones, 7-terminal
Pl ₁ , Pl ₂ , Pl ₃	Indicator lights, Drake No. 110-022 (Hi Brite)
S ₂	Switch, DPDT, Cutler-Hammer No. 8834K5
S _{3AB}	Switch, 4PDT, Cutler-Hammer No. 8838K4
T _{S2}	Terminal strip, Cinch-Jones, 6-terminal

The servo-system gain is adjusted with the internal gain control in the servo amplifier. The gain must be high enough to get the desired accuracy in rate. However, as gain is increased, the system may oscillate. The damping network suppresses this oscillation to some extent, allowing higher gain before oscillation begins. The optimum gain is just below the oscillation point and must be set experimentally. Usually, there will be a wide range of gain that will satisfy the two requirements of small error (high gain) and no oscillation (low gain).

Mounted adjacent to the servo amplifier on the front panel of the rate-control electronics chassis are the controls for selecting manual or automatic variation in evaporator voltage and for operating the servo variac with a manual switch. These controls are used to set up the initial condition of evaporator voltage.

The rate detector, reference oscillator and mixer, rate programmer, servo amplifier, and motor variac controls comprise the rate controller electronics and are mounted on a single chassis. Figures C-15, C-16, and C-17 are photographs of the assembled electronics.

Power control panel

The Power Control Panel houses the servo driven variac, a manual range setting variac and a transformer which are connected to provide the desired range of voltage to the evaporator unit. Figure C-18 is a schematic of the power panel and the following page is the parts list; Figures C-19 and C-20 are photographs of the assembled panel.

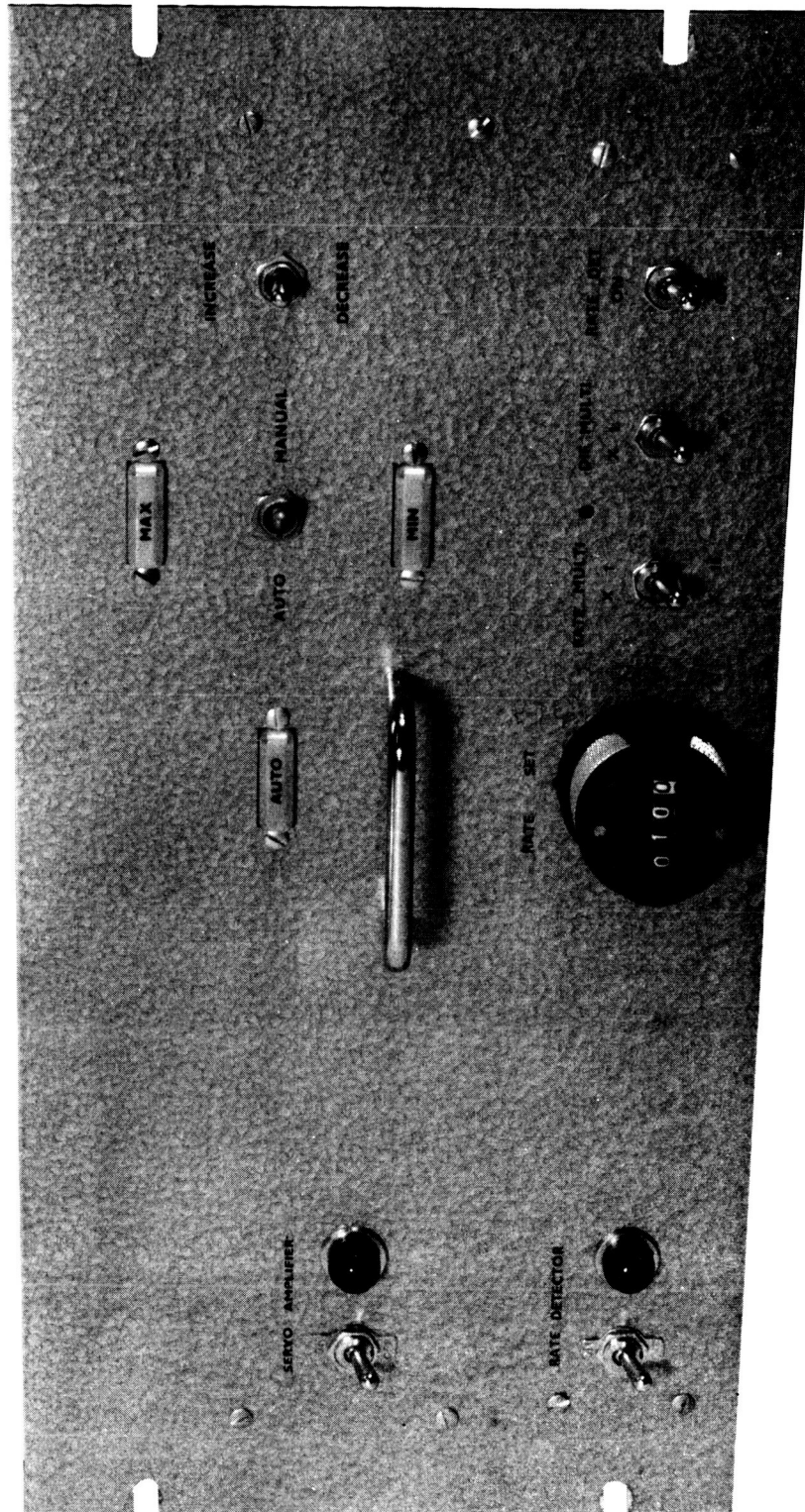


Figure C-15. Rate Controller, Front View

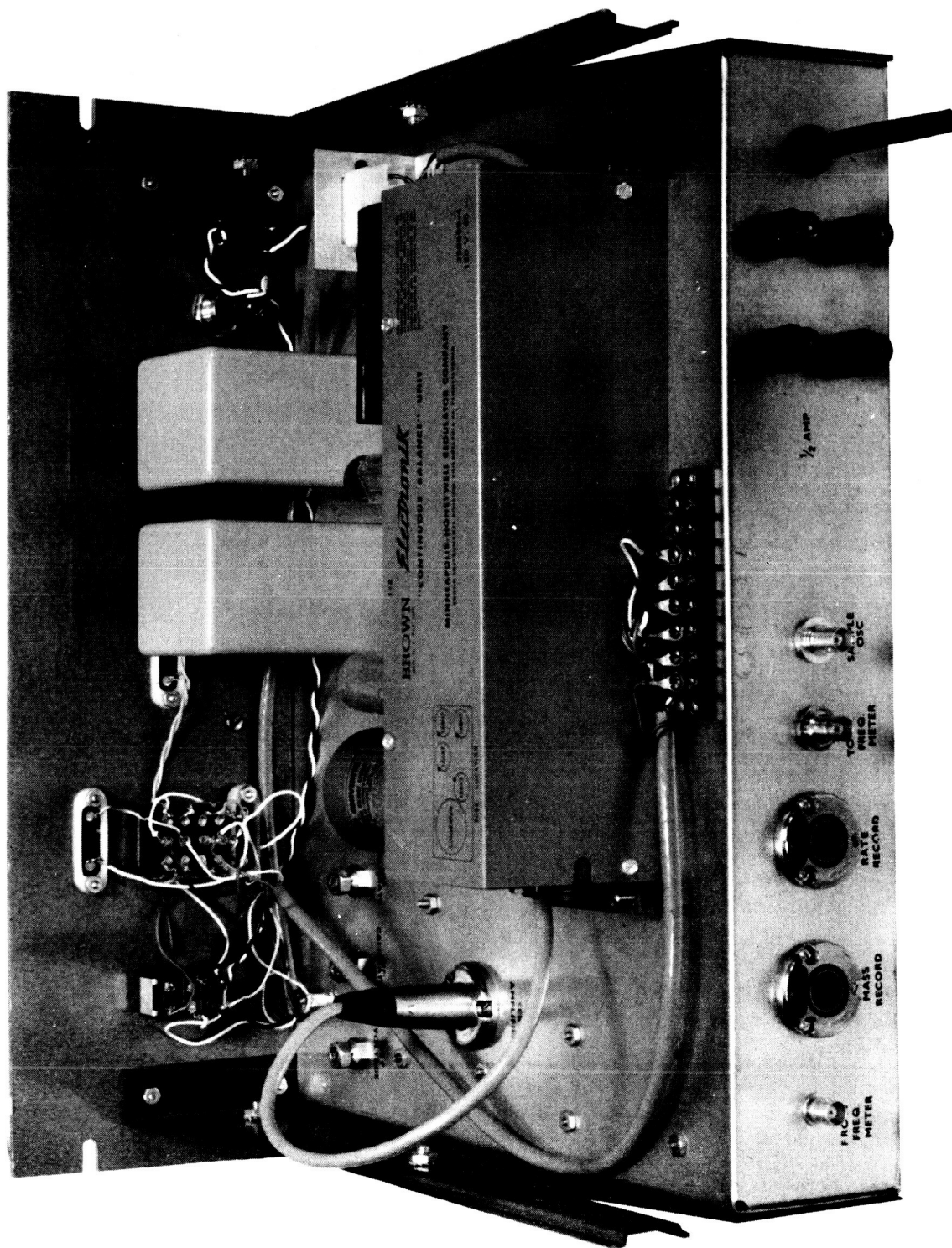


Figure C-16. Rate Controller, Rear View

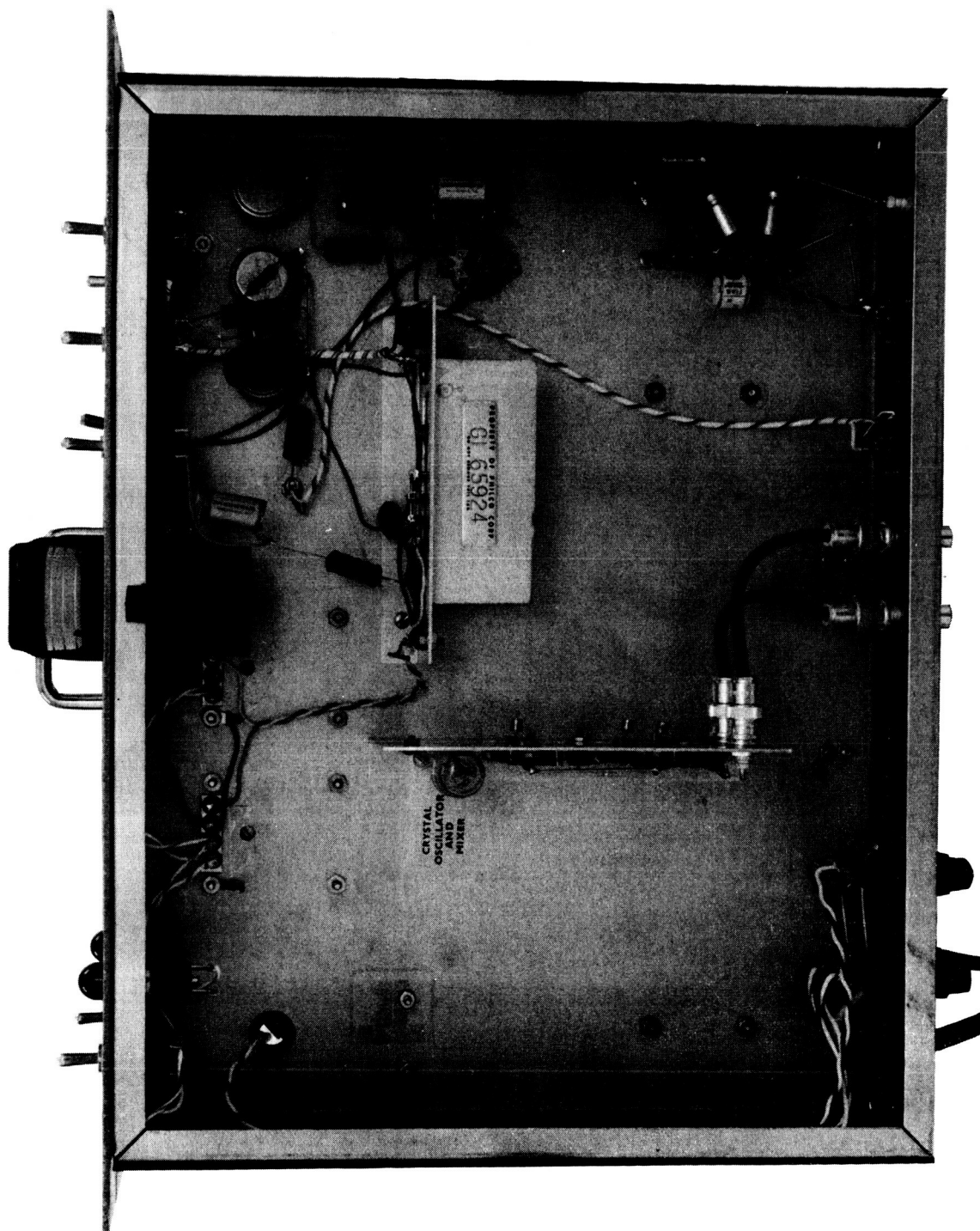
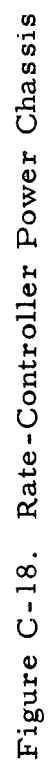


Figure C-17. Rate Controller, Bottom View



Parts List for Rate Controller Power Chassis
(Figure C-18)

Symbol	Description
CB ₁	Circuit breaker, 10-ampere, Wood Electric No. 190-210-101
Pl ₁	Pilot light, Dialight No. 514001-211
VM ₁	Variac, motor-driven, General Radio No. W10D128CKM
V ₁	Variac, Superior Electric Co., No. 116U
M ₁	Meter, 150 vac, 3-1/2 inch, Simpson No. 1357
M ₂	Meter, select to match evaporator voltage
T ₁	Transformer, multitap, high current, sec 12 amperes, 2 windings, 18 volts
T _{S1}	Terminal strip, Cinch-Jones No. 3-140Y
T _{S2}	Terminal strip, Cinch-Jones No. 3-140Y
G _{P1}	Parallel ground plug, male
G _{P2}	Connector, chassis, 3-wire ac, male

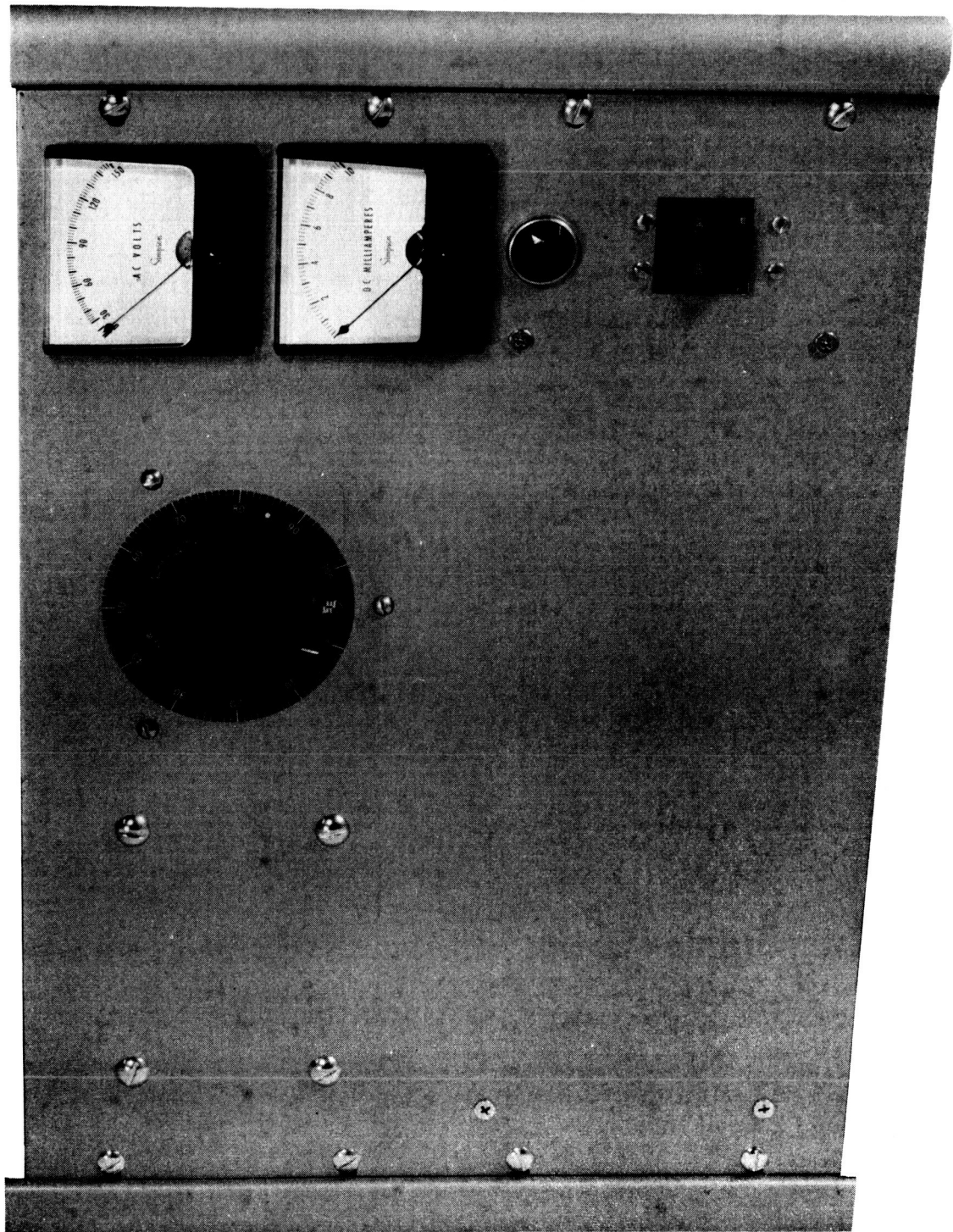


Figure C-19. Power Panel, Front View

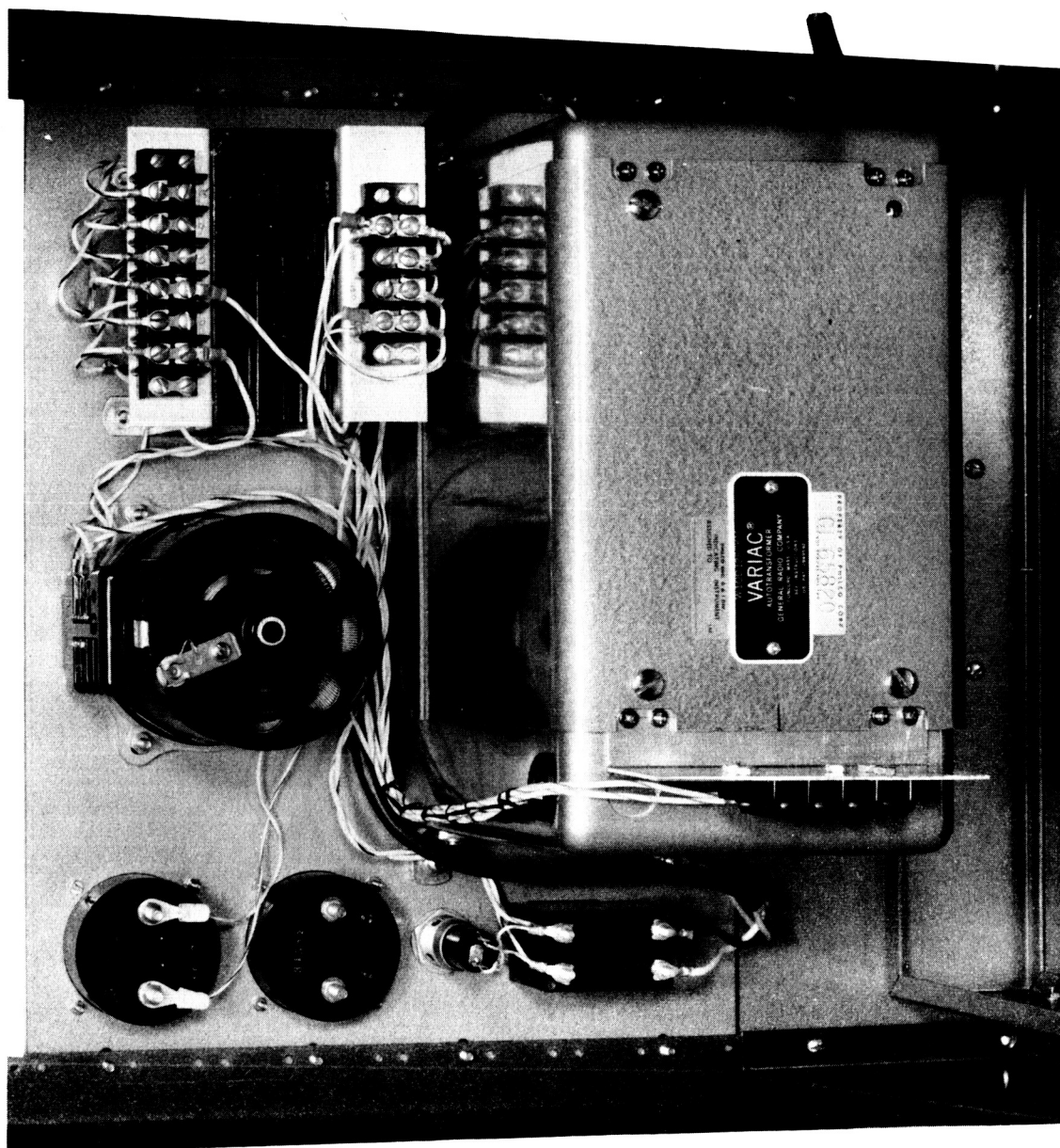


Figure C-20. Power Panel, Rear View

REFERENCES

1. Miles and Smith, "The Formation of Metal Oxide Films Using Gaseous and Solid Electrolytes," submitted to J. Electrochem. Soc.
2. Da Silva, E.M. and White, P., "Electrical Properties of Evaporated Aluminum Oxide Films," J. Electrochemical Soc., Vol. 109, No. 1, January 1962, p. 12.
3. Spratt, J.P., Final Report, Thin Film Active Devices, Contract No. DA-49-186-ORD-1056.
4. Kennard, E.H., Kinetic Theory of Gases, McGraw-Hill, New York.
5. Sauerbrey, G., Z. Physik, 155, 206, 1959.
6. Warner, A.W. and Stockridge, C.D., "Mass and Thermal Measurement With Resonating Crystalline Quartz," Vacuum Microbalance Techniques, Plenum Press, Vol. 2, 1961 pp. 71 to 92.
7. Berhardt and Love, Vac. Sys. Trans. p. 87, 1960; also Vacuum, pp. 1 to 9, Vol. 12, January-February 1962.

ABSTRACT

This report describes experimental and theoretical work on two areas of study regarding the production of radiation-resistant thin-film active devices.

An experimental and theoretical program is being pursued to determine the mean free path of energetic electrons obtained from a specially designed electron gun and injected into the metal surface-barrier contact of a metal semiconductor diode.

Aluminum oxide obtained by evaporating aluminum in a low-pressure oxygen environment will be studied with regard to electrical properties pertinent to the production of thin-film devices. The resistivity of the aluminum oxide can be controlled by variation in the oxygen pressure and deposition rate between the limits imposed by pure aluminum and pure aluminum oxide.